

The s-process enriched star HD 55496: origin from a globular cluster or from the tidal disruption of a dwarf galaxy? ^{*}

C.B. Pereira^{1†}, N. A. Drake^{1,2,3‡}, F. Roig^{1§}

¹ *Observatório Nacional/MCTIC, Rua Gen. José Cristino, 77, 20921-400, Rio de Janeiro, Brazil*

² *Laboratory of Observational Astrophysics, Saint Petersburg State University, Universitetski pr. 28, Petrodvoretz 198504, Saint Petersburg, Russia*

³ *Laboratório Nacional de Astrofísica/MCTIC, Rua Estados Unidos, 154, 37500-000, Itajubá, Brazil*

Accepted xxx. Received xxx; in original form xxxx

ABSTRACT

We present a new abundance analysis of HD 55496, previously known as a metal-poor barium star. We found that HD 55496 has a metallicity $[\text{Fe}/\text{H}] = -1.55$ and is s-process enriched. We find that HD 55496 presents four chemical peculiarities: (i) a Na-O abundance anti-correlation; (ii) it is aluminum rich; (iii) it is carbon poor for a s-process enriched star and (iv) the heavy 2nd s-process peak elements, such as Ba, La, Ce, and Nd, present smaller abundances than the lighter s-process elements, such as Sr, Y and Zr, which is not usually observed among the chemically-peculiar binary stars at this metallicity. The heavy-element abundance pattern suggests that the main source of the neutrons is the $^{22}\text{Ne}(\alpha, n)^{25}\text{Mg}$ reaction. Taken all these abundance evidence together into consideration, this strongly suggests that HD 55496 is a “second generation of globular cluster star” formed from gas already strongly enriched in s-process elements and now is a field halo object. Our dynamical analysis, however, indicates that the past encounter probabilities with the known globular clusters is very small ($\leq 6\%$). This evidence, together with the fact of having a retrograde motion, points to a halo intruder possibly originated from the tidal disruption of a dwarf galaxy.

Key words: nuclear reactions, nucleosynthesis — stars: abundances — stars: individual: HD 55496 stars: chemically peculiar — stars: evolution — stars: fundamental parameters

1 INTRODUCTION

It is well known that “second generation of globular cluster stars” present an anti-correlation of the abundances among the light elements, such as a depletion of carbon, oxygen and magnesium accompanied by an overabundance of other light elements, such as sodium, aluminum and nitrogen (e.g. Shetrone 1996, Carretta et al. 2010, just to name a few of the many works dedicated to investigate the chemical abundances in globular clusters). Such abundance pattern or the anti-correlations between these abundances have not been observed in the past among the stars of the halo of low metallicity. Thus, any star found in the field halo in the Galaxy presenting such abundance pattern could be considered as a second generation candidate star of a globular cluster that has escaped from the cluster (Fernández-Trincado et al. 2016, Carretta et al. 2010). Finding these kind of stars within field halo of the Galaxy is not an easy task and few of them have been found in the last years, thanks to large spectroscopic surveys (Ramírez et al. 2012; Schiavon et al. 2017; Fernández-Trincado, 2016, 2017, Martell et al. 2016), and to photometric plus dynamical analysis searching for tidal debris from ω Cen (Majewski et al. 2012).

In this work we present a new abundance and dynamical analysis of the star HD 55496. This star, first noticed as a barium star by MacConnel et al. (1972) and later classified as a “metal-poor barium star” by Luck & Bond (1991), was observed during the high-resolution spectroscopic survey dedicated to investigate and to determine the heavy-abundance abundance pattern of a sample of barium stars. Barium stars represent among the chemically peculiar stars the largest sample, and therefore they are useful targets to constrain nucleosynthesis process in the asymptotic giant branch (AGB) stars (de Castro et al. 2016, Cseh et al. 2018). Being a barium star, HD 55496 should also be a binary star, but analysis of radial velocity data collected over 14 years were inconclusive (Jorissen et al. 2015).

As we shall see, HD 55496 is an atypical object to be classified as a barium star. Not

* Based on the observations made with the 2.2m telescope at the European Southern Observatory (La Silla, Chile) under the agreement between Observatório Nacional (Brazil) and European Southern Observatory (ESO)

† E-mail:claudio@on.br

‡ E-mail:drake@on.br

§ E-mail:froig@on.br

only due to the inconclusive results of the radial velocity variation, but also due to its peculiar chemical abundance of the elements created by the *s*-process and the high sodium and aluminum abundances. This chemical peculiarity, turns HD 55496 to be an attractive object for an investigation whether it can be a “second generation of globular cluster star” which is now a field halo object.

This work is organized as follows: In Section 2 we describe the observations. In Section 3 we describe the determination of the atmospheric parameters and the chemical abundances. In Section 4, we discuss the results obtained for the luminosity, for the radial velocity, for the chemical abundances and for the kinematical analysis. Finally, our conclusions are presented in Section 5.

2 OBSERVATIONS

The high-resolution spectrum of HD 55496 was obtained with the FEROS (Fibre-fed Extended Range Optical Spectrograph) echelle spectrograph (Kaufer et al. 1999) at the 2.2 m ESO telescope in La Silla (Chile), during the night of April 3, 2007. The exposure time for this observation was 900 sec. Technical details about the FEROS spectrograph is reported in Santrich et al. (2013).

Since HD 55496 has a high sodium and aluminum abundance it is important to compare the spectrum of HD 55496 with another star whose atmospheric parameters are similar to that of HD 55496 and not either sodium nor aluminum enriched. In this case, the differences in the strengths of absorption lines of sodium and aluminum between the two stars will be only due to a high abundance of sodium and aluminum in HD 55496. Figures 1, 2 and 3 show the spectra of HD 55496 in the spectral regions of the interest of the present work, that is around the Na I and Al I absorption lines in comparison with the spectrum of CD-27°8864. CD-27°8864, is a metal-poor star with similar effective temperature ($T_{\text{eff}} = 4650$ K), surface gravity ($\log g = 1.6$), iron abundance ($[\text{Fe}/\text{H}] = -1.54$), and microturbulent velocity 1.6 km s^{-1} analyzed in Pereira et al. (2019).

3 ANALYSIS

3.1 Atmospheric Parameters

For the determination of the atmospheric parameters it is first necessary to measure the equivalent widths of the absorption lines of Fe I and Fe II. The absorption lines selected for

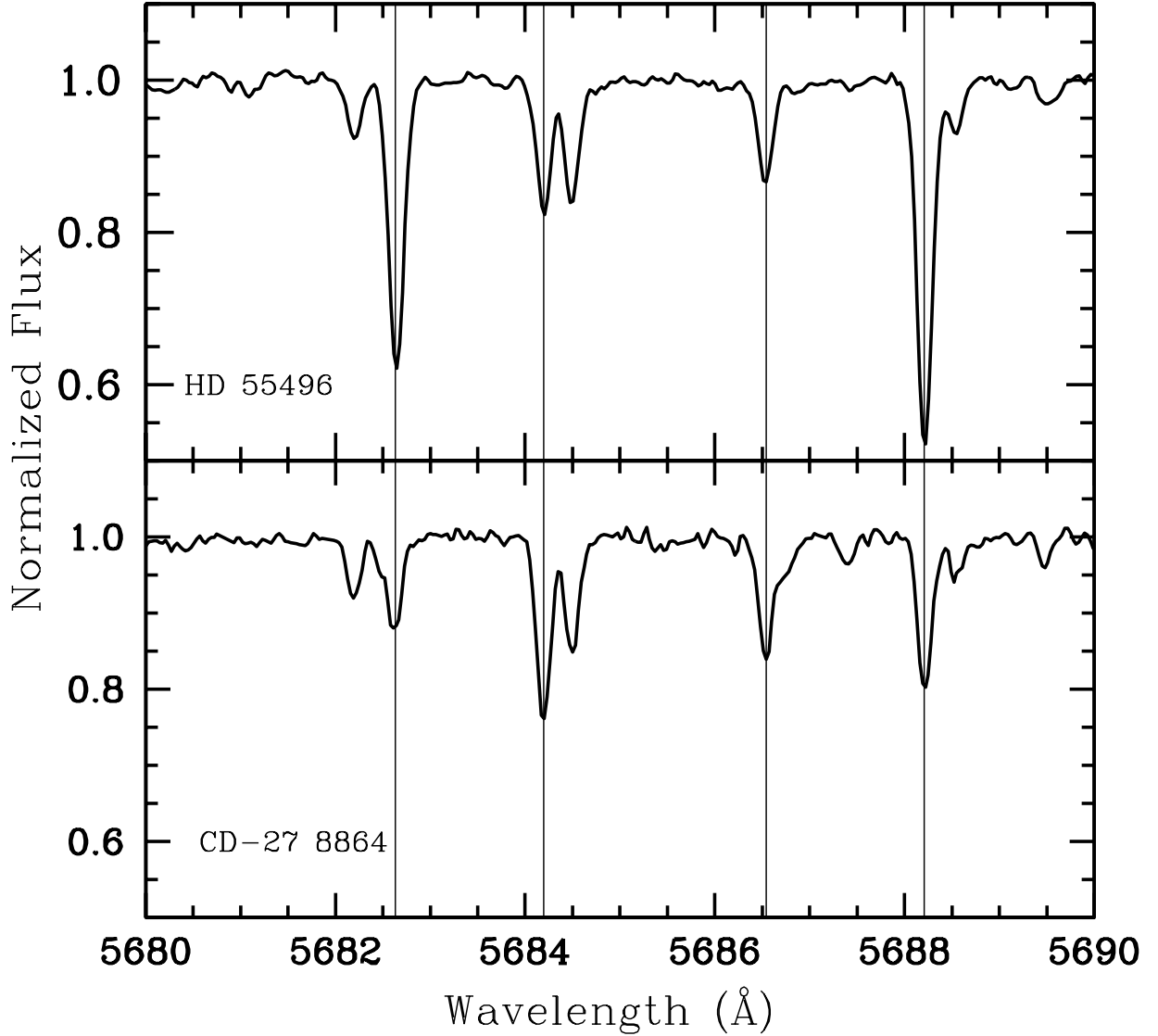


Figure 1. Spectra of HD 55496 and CD-27°8864 between 5680 and 5690 Å. Vertical lines represent the transitions of Na I 5682.65, Sc II 5684.20, Fe I 5686.54 and Na I 5688.22 Å. We show the spectra of CD-27°8864 because it has similar temperature, surface gravity and metallicity of HD 55496.

this task were selected from Lambert et al. (1996) and that was the same source of lines used in the work of Moriz et al. (2017) in the study of the CD-50°776 recently identified as a new CEMP-s.¹ Table 1 shows the values of the equivalent widths of the Fe I and Fe II absorption lines with their respective excitation potentials (χ in eV) and the $\log gf$ values of the transitions. The equivalent widths were determined using the *splot* task in IRAF by adjusting Gaussian profiles to the observed profiles.

¹ CEMP stands for Carbon-Enhanced Metal-Poor. The suffix "s" means that the star is s-process enriched.

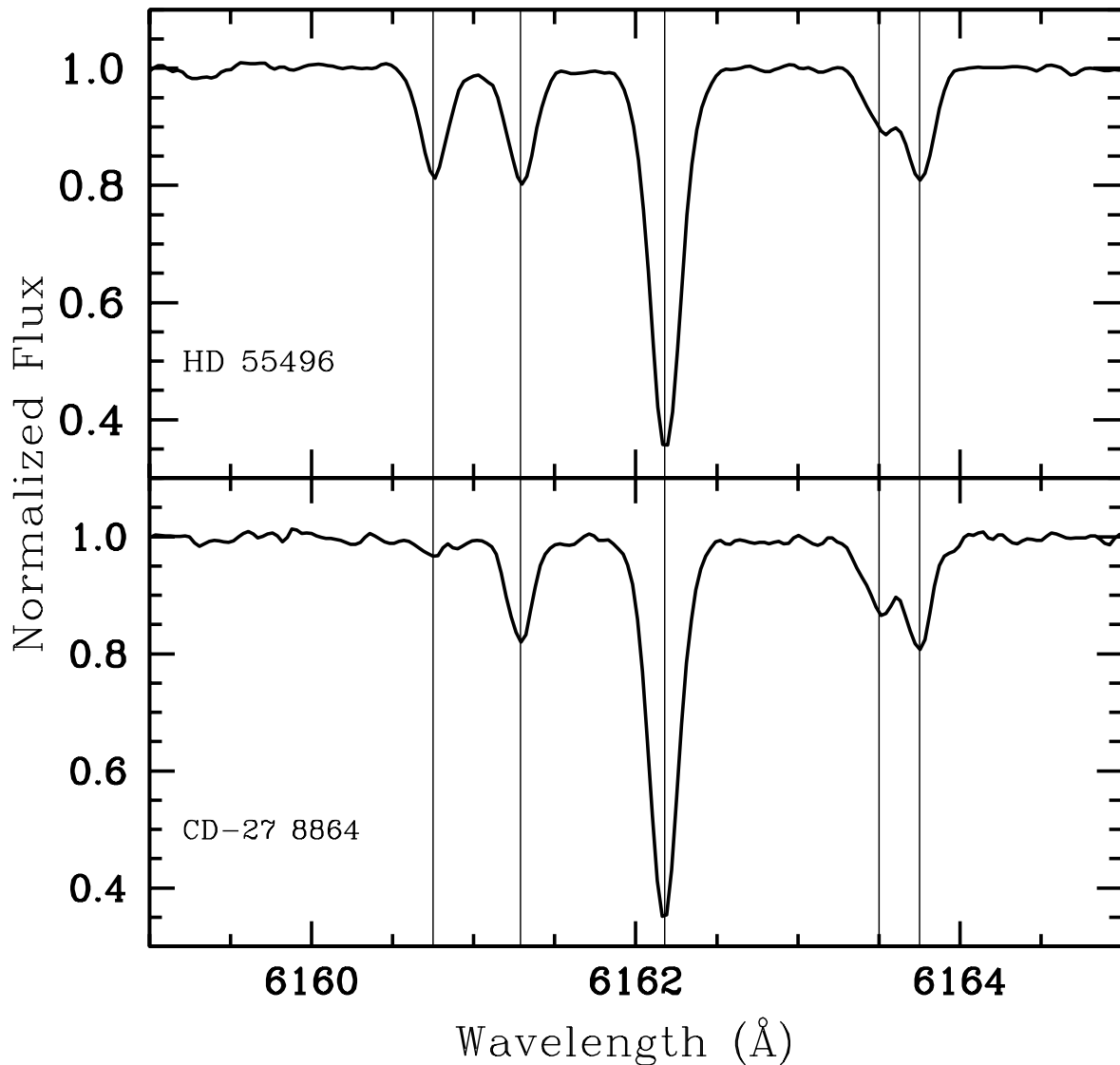


Figure 2. Same as Figure 1 but for the spectral region between 6159 and 6165 Å. Vertical lines represent the transitions of Na I 6160.73, Ca I 6161.27, 6162.18 and Fe I 6163.55 and Ca I 6163.75 Å.

In addition, the determination of the stellar atmospheric parameters, such as effective temperature (T_{eff}), surface gravity ($\log g$), microturbulence (ξ), and metallicity ($[\text{Fe}/\text{H}]$) (we use the notation $[\text{X}/\text{H}] = \log(N_{\text{X}}/N_{\text{H}})_{\star} - \log(N_{\text{X}}/N_{\text{H}})_{\odot}$), were also done in the same way as in Roriz et al. (2017). In brief, it consists in using the local thermodynamic equilibrium (hereafter LTE) model atmospheres of Kurucz (1993) and the spectral analysis code MOOG, version 2013 (Snedden 1973). Table 2 shows the final adopted atmospheric parameters with their respective errors. Previous atmospheric parameters determination for HD 55496 were

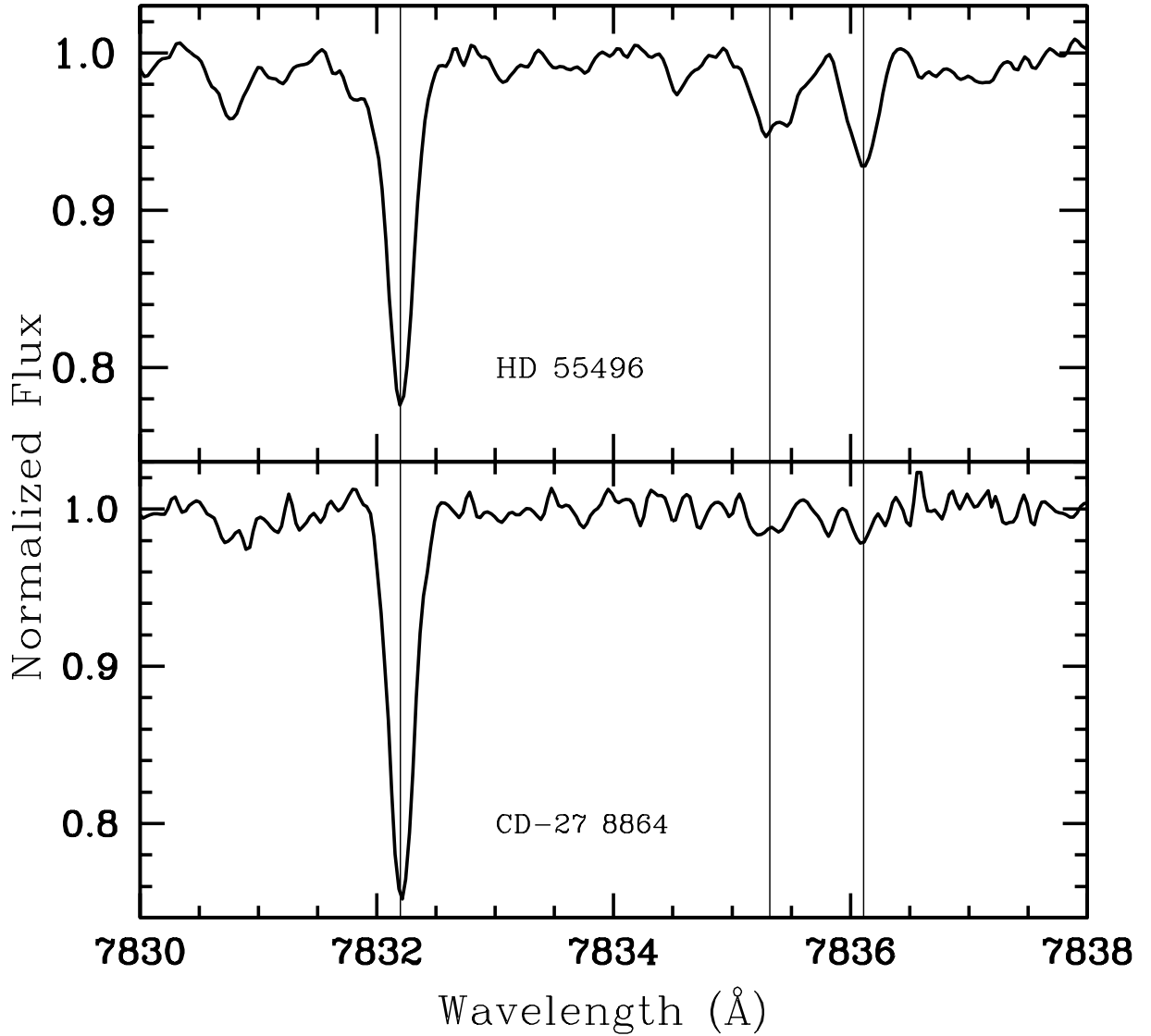


Figure 3. Same as Figure 1 but for the spectral region between 7830 and 7838 Å. Vertical lines represent the transition of Fe I at 7838.21 Å and the Al I transitions at 7835.32 and 7836.13 Å.

obtained by Karinkuzhi & Goswami (2015) and earlier by Luck & Bond (1991). Our results are similar to those of Karinkuzhi & Goswami (2015).

The errors in temperature and microturbulent velocity were estimated considering, respectively, the uncertainty in the value of the slope of the relationships between the abundance of iron, given by the Fe I lines, and the excitation potential and the abundance of iron and the reduced equivalent width. For gravity, the uncertainty was estimated considering that the difference between the Fe I and Fe II abundances differed by 1σ of the standard deviation of the mean value of Fe I abundances. We found for the temperature, surface grav-

Table 2. Atmospheric parameters for HD 55496.

Parameter	Value	Ref.
T_{eff} (K)	4700 ± 70	1
	4850	2
	4800	3
	4750	4
$\log g$ (dex)	1.9 ± 0.2	1
	2.05	2
	2.8	3
	2.5	4
[Fe/H] (dex)	-1.55 ± 0.11	1
	-1.49	2
	-1.55	3
ξ (km s ⁻¹)	1.5 ± 0.3	1
	1.5	2
	2.7	3
	1.5	4

References for Table 2.

- 1: This work;
2: Karinkuzhi & Goswami (2015);
3: Luck & Bond (1991);
4: Sneden (1983);

ity and for the microturbulent velocity uncertainties of $\sigma(T_{\text{eff}}) = \pm 70$ $\sigma(\log g) = \pm 0.2$ and $\sigma(\xi) = \pm 0.3$ km s⁻¹, respectively.

3.2 Abundance analysis

The abundances of chemical elements Na, Mg, Al, Si, Ca, Ti, Cr, Ni, Sr, Y, Zr, Mo, Ce, Nd and Sm were determined by measuring the equivalent widths of their absorption lines considering local-thermodynamic-equilibrium (LTE) model-atmosphere. We used the line-synthesis code MOOG, (Sneden, 1973) for the calculations and Table 3 shows the atomic lines used to obtain the abundances of the elements and Table 4 provides the results, the number of lines employed for each species, n , and the standard deviations. Our abundances were determined differentially with respect to the solar abundances of Grevesse & Sauval (1998).

The abundances of carbon, nitrogen, oxygen and lithium were determined by means of the spectral synthesis technique. For carbon, the abundance was determined using the CH lines of the $A^2\Delta - X^2Pi$ system at $\sim 4365 \text{ \AA}$. For the determination of the abundance of nitrogen and the $^{12}\text{C}/^{13}\text{C}$ isotopic ratio, we used the ^{12}CN lines of the (2, 0) band of the CN red system $A^2\Pi - X^2\Sigma$ in the 7994 – 8020 Å wavelength range. For the abundance of oxygen, we used the forbidden line at 6300.3 Å where we adopted $\log gf = -9.72$ from Allende Prieto et al. (2001). The lithium abundance was derived using the Li I λ 6708 Å resonance doublet.

The oscillator strengths and wavelengths of the CH and CN molecular lines and the

Table 4. Elemental abundances derived for HD 55496. The second column provides the solar abundances. The third column gives the information whether abundances were determined using spectrum synthesis technique (syn) or based on the equivalent width measurements. In this latter case we provide the number of lines (n) used for the abundance determination. The fourth and fifth columns give, respectively, the abundance in the scale $\log \varepsilon(\text{H}) = 12.0$ with the respective abundance dispersion among the lines of the elements with more than three available lines. The sixth and the seventh columns give the abundances in the notations $[\text{X}/\text{H}]$ and $[\text{X}/\text{Fe}]$. For the elements Sr, Mo and Pb the abundance dispersion was calculated considering three different positions of the continuum.

Species	$\log \varepsilon^{\odot}$	n(#)	$\log \varepsilon$	σ_{obs}	$[\text{X}/\text{H}]$	$[\text{X}/\text{Fe}]$
Li	3.31	syn	0.00	0.15	—	—
C (CH)	8.52	syn	6.62	0.05	-1.90	-0.35
N (CN)	7.92	syn	8.17	0.05	+0.25	+1.80
O	8.83	syn	7.43	0.10	-1.40	+0.15
Na I	6.33	8	5.59	0.13	-0.74	+0.81
Mg I	7.58	5	6.73	0.14	-0.85	+0.70
Al I	6.47	6	5.66	0.12	-0.81	+0.74
Si I	7.55	6	6.66	0.09	-0.89	+0.66
Ca I	6.36	16	5.39	0.12	-0.97	+0.58
Ti I	5.02	24	3.72	0.07	-1.30	+0.25
Fe I	7.50	70	5.95	0.11	-1.55	—
Fe II	7.50	10	5.92	0.09	-1.58	—
Cr I	5.67	10	4.06	0.11	-1.61	-0.06
Ni I	6.25	35	4.70	0.09	-1.55	0.00
Sr I	2.97	1	2.04	0.07	-0.93	+0.62
Y II	2.24	7	1.53	0.13	-0.71	+0.84
Zr I	2.60	6	2.20	0.06	-0.40	+1.15
Zr II	2.60	4	2.28	0.06	-0.32	+1.23
Mo I	1.92	1	1.47	0.10	-0.45	+1.10
Ba II	2.13	syn	1.20	0.06	-0.93	+0.62
La II	1.17	syn	-0.07	0.08	-1.24	+0.31
Ce II	1.58	10	0.54	0.10	-1.04	+0.51
Nd II	1.50	21	0.34	0.10	-1.16	+0.39
Sm II	1.01	6	-0.35	0.06	-1.36	+0.19
Pb I	1.95	syn	1.75	0.05	-0.20	+1.35

Li I doublet were taken from Drake & Pereira (2008). For the other elements which were abundances were determined using spectral synthesis, such as barium, lanthanum, and lead, the line lists were constructed using the databases of Kurucz² and VALD.³ Figures 4, 5 and 6 show the observed and synthetic spectra for the spectral regions where the abundances of carbon, nitrogen and lead were obtained.

The abundances of barium, lanthanum and lead were also determined by means of the spectral synthesis technique. The determination of barium abundance was obtained using the Ba II lines at $\lambda 4554.0$, $\lambda 4934.1$ and $\lambda 5853.7$. Hyperfine and isotope splitting were taken from McWilliam (1998) and the lead abundance was derived from the Pb I line at $\lambda 4057.81 \text{ \AA}$ where the isotopic shifts and hyperfine splitting were taken from van Eck et al. (2003). For lanthanum, the abundance was determined using the La II lines at $\lambda 4086.7$, $\lambda 4662.5$, $\lambda 5114.5$ and $\lambda 5303.5$ where the isotopic shifts and hyperfine splitting were taken from Roederer & Thompson (2015) and Karinkuzhi et al. (2018).

² <http://kurucz.harvard.edu/>

³ <http://vald.astro.uu.se/>

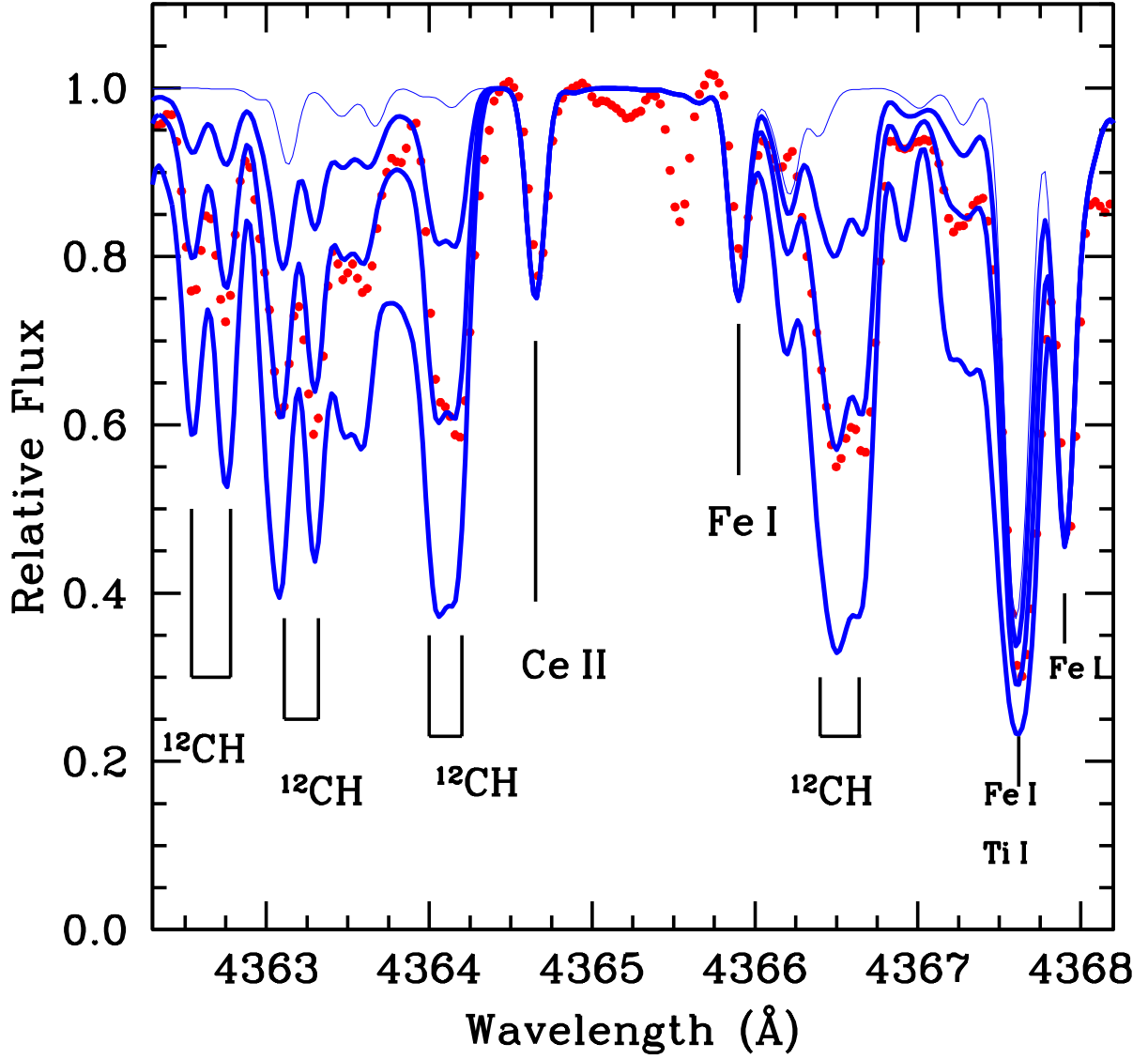


Figure 4. The observed spectrum of HD 55496 (red dots) and synthetic spectra in the spectral region between 4362.3 \AA and 4368.2 \AA where we can see the CH molecular lines. The lighter blue line shows the synthetic spectrum calculated without the contribution of the CH molecular lines. Blue solid lines, from top to bottom, show three synthetic spectra calculated respectively for the carbon abundances equal to $\log\epsilon(\text{C}) = 6.12, 6.62$ (adopted in this work) and 7.12 . Other absorptions lines are also showed.

3.3 Abundance uncertainties

Table 5 shows the uncertainties in the abundances of the chemical elements due to errors in temperature, surface gravity, microturbulence and metallicity determined previously in Section 3.1. Abundance errors were estimated by changing these parameters individually according to the uncertainties shown in Table 2. The uncertainties in the measurements of equivalent widths were estimated using the expression given by Cayrel (1988). For the

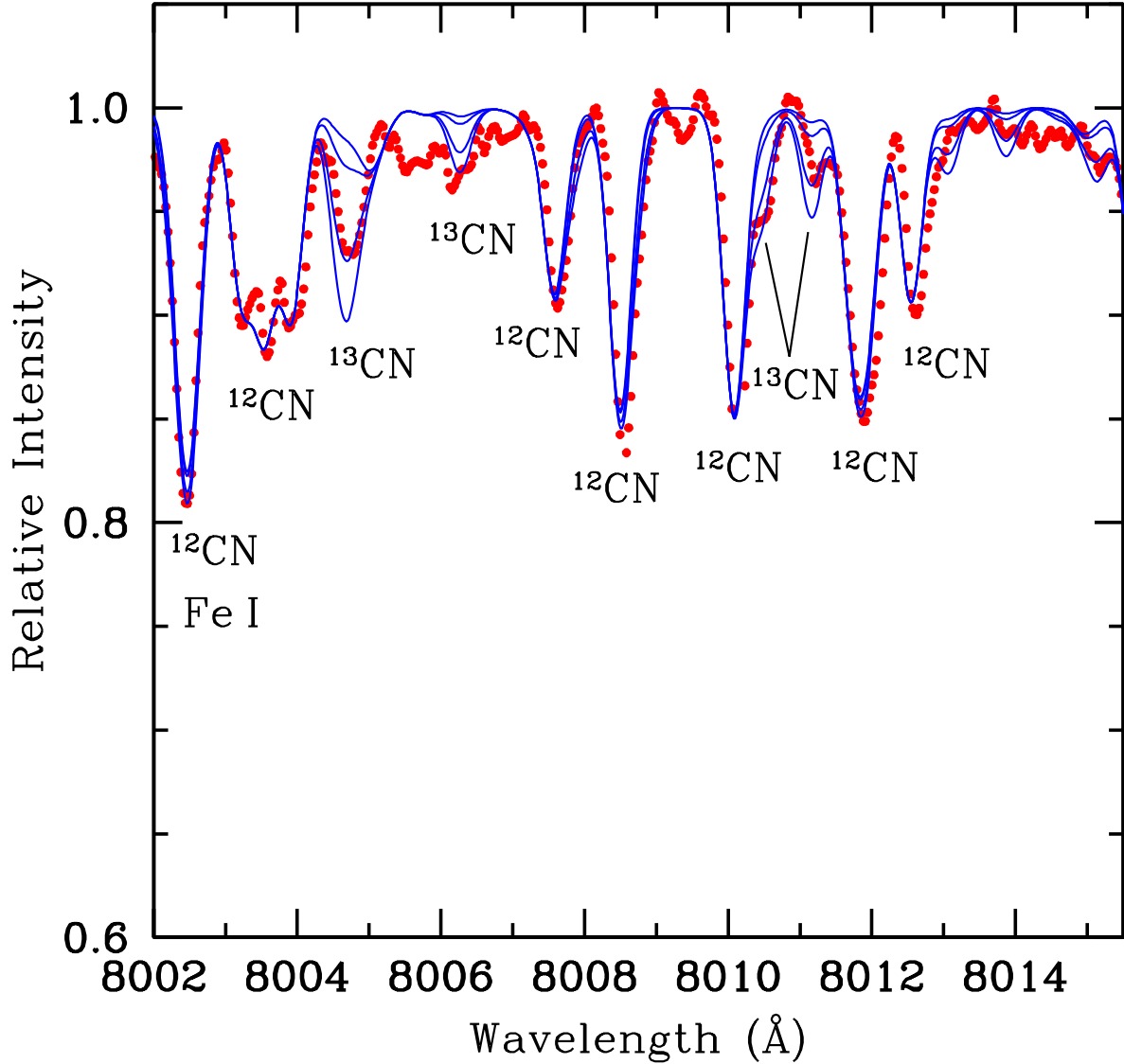


Figure 5. Observed (dotted red points) and synthetic (solid blue lines) spectra between λ 8002 and λ 8014.5 Å. From top to bottom we show the syntheses for four values of the $^{12}\text{C}/^{13}\text{C}$ isotopic ratio (36.0, 18.0, 6.0, and 4.0) and for $\log \varepsilon(\text{C}) = 6.62$, $\log \varepsilon(\text{N}) = 8.17$ (adopted) and $\log \varepsilon(\text{O}) = 7.43$. Other ^{12}CN absorptions are also indicated.

Feros spectrum having a nominal resolution of 48 000 and a S/N around 100, the estimated error is of the order of $3 \text{ m}\text{\AA}$. These error estimates were then taken into account in the measurements of the equivalent widths of the absorption lines of the chemical elements, providing other values for the elemental abundances. The eighth column of Table 5 shows the final uncertainty due to uncertainties in atmospheric parameters (temperature, surface gravity, metallicity and microturbulence velocity), equivalent widths and the dispersion of the abundances. The total uncertainty was calculated as the root quadratic sum of each of these parameters considering that each individual uncertainty is independent.

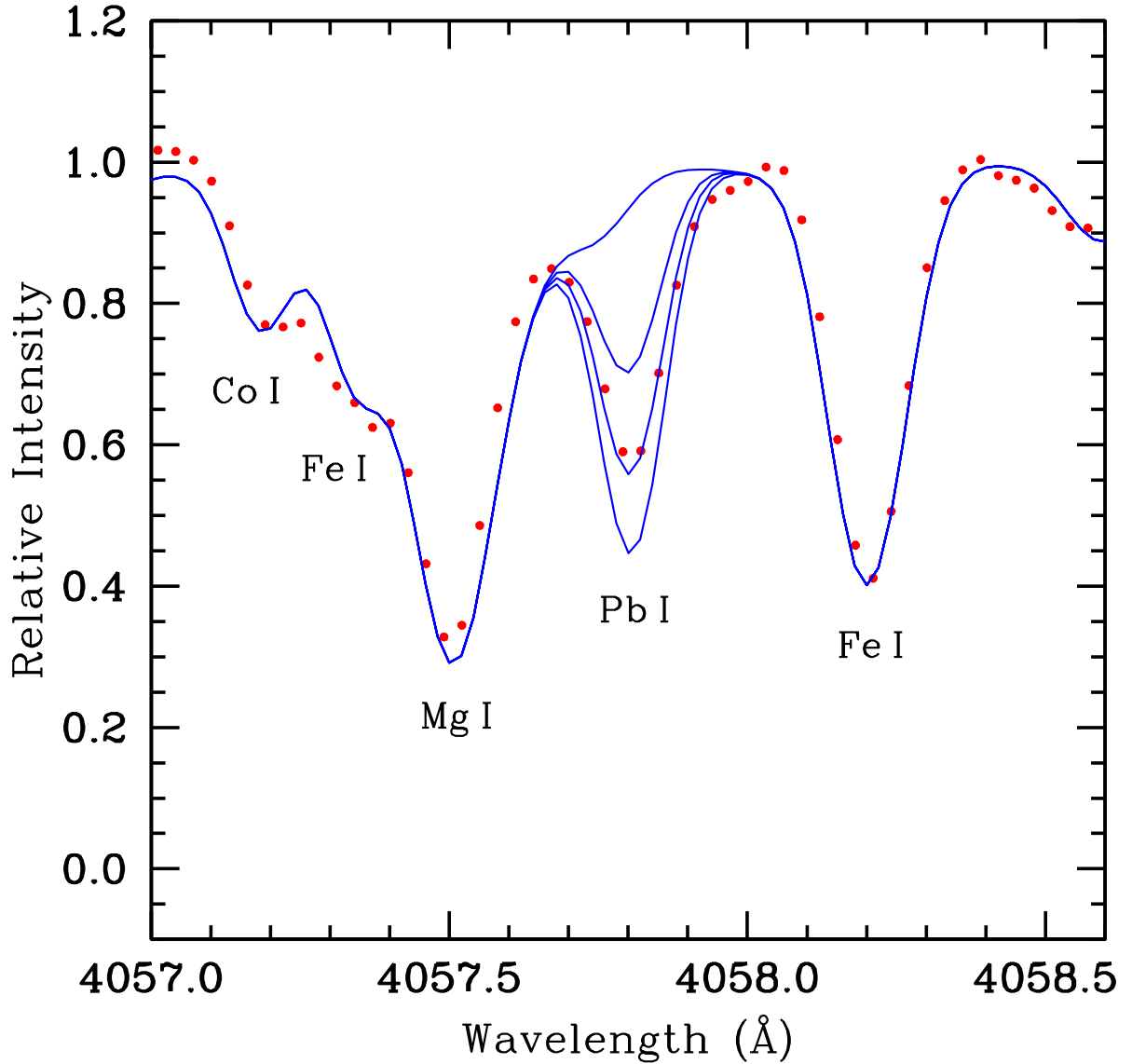


Figure 6. The observed spectrum of HD 55496 (red dots) in the spectral region between 4057.0 Å and 4058.6 Å where we can see the transition of Pb I at 4057.8 Å. Synthetic spectra (solid blue lines) are also shown calculated respectively for the lead abundances equal to $\log \epsilon(\text{Pb}) = 1.25, 1.75$ (adopted in this work) and 2.25. The lighter blue line shows the synthetic spectrum calculated without the contribution of the lead. Other absorptions lines are also showed.

For the elements analyzed through spectral synthesis technique we used the same methodology that was used to calculate the uncertainties of the abundances obtained based on measurements of the equivalent widths. We vary the temperature, surface gravity, metallicity and microturbulence velocity and then compute independently the variation of the abundances obtained by each value. In addition, for carbon, nitrogen and oxygen, we consider that their respective abundances are interdependent, that is, the uncertainty in the determination of abundance of oxygen affects the abundance of carbon and vice-versa. The uncertainties in

carbon abundance also affect the abundance of nitrogen since the CN molecule was used for the determination of nitrogen abundance. For the light elements, carbon, nitrogen and oxygen, the variations of the abundance due to changes in effective temperature, surface gravity and micro-turbulent velocities are given in Table 6. Abundances based on molecular lines are little affected by microturbulence velocity variation because they are weak lines. As for surface gravity, the molecules can be affected since the molecular equilibrium is sensitive to the gas pressure. However, considering variations of only 0.2 dex for the surface gravity, the error introduced in abundance is not significant. In fact similar uncertainties were found by Tautvaišienė et al. (2000).

Table 5 shows the well known behavior that the neutral elements are more sensitive to the temperature variations, while singly-ionized elements are more sensitive to the surface gravity variations (Gray 1992). For the elements whose abundance is based on stronger lines, such as strontium, yttrium and calcium the error introduced by the microturbulence is important. This is because the equivalent widths of the moderately strong lines which lie in the saturated part of the curve of growth are larger than those synthetic lines calculated considering only thermal and damping broadening. Once microturbulent velocity is introduced in the line computation, it delays the saturation of an absorption line in the curve of growth and also becomes the major source of uncertainty in the abundance analysis based in these strong lines. For stronger absorption lines with saturated cores, the wings grow increasing the line strength and become responsible for the most of their equivalent widths. Since the equivalent width is also proportional to the Doppler broadening which is related to microturbulent velocity, one should expect that microturbulence also affects the line strength.

4 RESULTS AND DISCUSSION

4.1 Luminosity

The luminosity of HD 55496 can be estimated based on the recently Gaia DR2 distance determination which is 494 ± 11 pc (Bailer-Jones 2018). Considering the relationship by Alonso et al. (1999) between bolometric correction (BC) and effective temperature, BC results to be -0.38 . Assuming $V = 8.4$ and $M_{\text{bol}\odot} = +4.74$ (Bessel, 1998), we obtain $\log(L_*/L_\odot) = 2.14 - 2.38$ or $L_* = 140 - 240 L_\odot$. This range in luminosity is due to uncertain interstellar absorption because the relatively low galactic latitude ($b = -5.96^\circ$) of HD 55496. In fact, using the cal-

Table 5. Abundance uncertainties for HD 55496. Second column gives $\sigma_{\log \varepsilon} = \sigma_{\text{obs}}/\sqrt{n}$ where n is the number of absorption lines used for the abundance determination. See fifth column of Table 4 for the values of σ_{obs} . Columns 3 to 7 give the variation of the abundances caused by the variation in T_{eff} , $\log g$, ξ , $[\text{Fe}/\text{H}]$, and equivalent width measurements (W_λ), respectively. The 8th column gives all the uncertainties quadratically combined from the 3rd to 7th columns. The last column gives the abundance dispersion observed among the lines for those elements with three or more lines available as already shown in Table 4.

Species	$\sigma_{\log \varepsilon}$	ΔT_{eff} $\pm 70 \text{ K}$	$\Delta \log g$ ± 0.2	$\Delta \xi$ $\pm 0.3 \text{ km s}^{-1}$	$\Delta [\text{Fe}/\text{H}]$ ± 0.1	ΔW_λ $\pm 3 \text{ m\AA}$	$(\sum \sigma^2)^{1/2}$	σ_{obs}
Li	0.15	+0.10/−0.10	+0.05/−0.05	0.00/0.00	0.00/0.00	—	0.19/0.19	0.15
Fe I	0.01	+0.09/−0.09	−0.01/+0.01	−0.11/+0.13	−0.01/+0.01	+0.07/−0.07	0.16/0.17	0.11
Fe II	0.03	−0.02/+0.04	+0.09/−0.07	−0.03/+0.05	+0.02/−0.01	+0.09/−0.09	0.10/0.12	0.09
Na I	0.05	+0.06/−0.06	−0.02/+0.02	−0.05/+0.05	−0.01/+0.01	+0.05/−0.06	0.09/0.11	0.13
Mg I	0.06	+0.07/−0.06	−0.04/+0.04	−0.07/+0.07	0.00/+0.01	+0.05/−0.04	0.11/0.12	0.14
Al I	0.05	+0.04/−0.05	−0.01/+0.01	−0.02/+0.02	−0.01/+0.01	+0.06/−0.07	0.09/0.10	0.12
Si I	0.04	+0.02/−0.01	+0.02/−0.01	−0.01/+0.02	0.00/0.00	+0.09/−0.10	0.10/0.11	0.09
Ca I	0.03	+0.07/−0.07	−0.03/+0.02	−0.12/+0.12	−0.02/+0.01	+0.06/−0.07	0.16/0.16	0.12
Ti I	0.01	+0.12/−0.13	−0.02/+0.02	−0.06/+0.07	−0.01/+0.02	+0.07/−0.07	0.15/0.17	0.07
Cr I	0.03	+0.10/−0.10	−0.02/+0.01	−0.08/+0.10	−0.01/+0.02	+0.08/−0.09	0.13/0.17	0.11
Ni I	0.01	+0.08/−0.09	−0.02/0.00	−0.05/+0.06	−0.01/0.00	+0.07/−0.08	0.12/0.13	0.09
Sr II	0.07	+0.12/−0.13	−0.03/+0.03	−0.17/+0.24	−0.02/+0.02	+0.08/−0.08	0.23/0.30	0.07
Y II	0.05	+0.02/−0.01	+0.06/−0.06	−0.17/+0.22	+0.02/−0.01	+0.08/−0.07	0.21/0.24	0.13
Zr I	0.02	+0.13/−0.13	−0.01/+0.02	−0.01/+0.02	0.00/+0.02	+0.10/−0.11	0.16/0.17	0.06
Zr II	0.03	+0.01/0.00	+0.07/−0.06	−0.13/+0.19	+0.02/−0.01	+0.08/−0.07	0.17/0.21	0.06
Mo I	0.10	+0.11/−0.12	−0.02/+0.01	−0.01/+0.01	−0.01/+0.01	+0.13/−0.18	0.20/0.24	0.10
Ba II	0.03	0.01/0.00	+0.10/−0.10	−0.20/+0.30	0.00/0.00	—	0.23/0.31	0.06
La II	0.04	−0.05/+0.05	+0.10/−0.10	0.00/0.00	0.00/0.00	—	0.12/0.12	0.08
Ce II	0.03	+0.02/−0.02	+0.08/−0.07	−0.05/+0.09	+0.02/−0.02	+0.08/−0.09	0.13/0.15	0.10
Nd II	0.02	+0.02/−0.03	+0.07/−0.08	−0.04/+0.05	+0.02/−0.03	+0.08/−0.09	0.12/0.14	0.10
Sm II	0.02	+0.03/−0.02	+0.08/−0.07	−0.02/+0.04	+0.03/−0.02	+0.09/−0.09	0.13/0.13	0.06
Pb I	0.05	+0.10/−0.20	0.00/0.00	−0.10/+0.10	0.00/0.00	—	0.11/0.22	0.05

Table 6. Abundance errors for the elements C, N, O of HD 55496.

Species	$\sigma_{\log \varepsilon}$	ΔT_{eff} $\pm 70 \text{ K}$	$\Delta \log g$ ± 0.2	$\Delta \xi$ $\pm 0.3 \text{ km s}^{-1}$	$\Delta \log (\text{C})$ $+0.20$	$\Delta \log (\text{N})$ $+0.20$	$\Delta \log (\text{O})$ $+0.20$	σ_{tot}
C	0.05	+0.10/−0.10	0.00/−0.05	0.00/0.00	—	0.00	+0.15	+0.19/+0.19
N	0.02	+0.10/−0.10	+0.05/−0.05	0.00/0.00	−0.10	—	+0.20	+0.29/+0.29
O	0.10(?)	+0.05/−0.05	+0.10/−0.10	0.00/−0.05	0.00	0.00	—	+0.15/+0.16

ibrations between A_V , galactic coordinates and distances given by Chen et al. (1998), we obtain $A_V = 0.16$ or 0.61 .

The luminosity above obtained is not enough for a star develop helium-burning through the thermal pulses during AGB phase and then becoming a star rich in elements formed by slow neutron capture. Theoretical calculations show that for a star to develop the first thermal pulse the required luminosity should be around $1800 L_\odot$ (Lattanzio, 1986) or $1400 L_\odot$ (Vassiliadis & Wood, 1993).

We can also estimate the distance through the derived effective temperature and surface gravity. The relation between the distance of a star to the Sun, r , and its temperature, gravity, mass, V magnitude, bolometric correction (BC), and interstellar absorption (A_V), is given by:

$$\log r \text{ (kpc)} = \frac{1}{2} \left(\log \frac{M_{\star}}{M_{\odot}} + 0.4 \times (V - A_V + BC) + 4 \times \log T_{\text{eff}} - \log g - 16.5 \right). \quad (1)$$

Using the values of the temperature and surface gravity given in Table 2 and the values of the V -magnitude and the bolometric correction given above and assuming a mass of $M = 0.8 M_{\odot}$ for HD 55496 (the low metallicity suggests an old and hence lower mass nature) equation (1) can be written as

$$\log r \text{ (kpc)} = \frac{1}{2} (-0.4 \times A_V - 0.6) \quad (2)$$

Considering the three possible values for the interstellar absorption above mentioned 0.16 and 0.61 the obtained distance is, respectively, 465 and 378 parsecs. The first value, obtained for $A_V = 0.16$ is in agreement with the recent distance determination of the Gaia DR2 release.

4.2 Radial Velocity

Table 7 shows all known measurements of radial velocity of HD 55496 available in the literature and determined in this work. We determined the radial velocity measuring the Doppler shifts of selected absorption lines. It is not clear whether the radial velocity of HD 55496 presents variations due to orbital motion. A similar conclusion has already been raised by Jorissen et al. (2005). In Figure 7 we show the radial velocity measurements obtained by Jorissen et al. (2005) where we also include our value of $315.63 \pm 0.23 \text{ km s}^{-1}$. It seems that there is no significant variation of the radial velocity. Systematic radial velocity monitoring is necessary to confirm the possible binary nature of HD 55496. If HD 55496 would indeed be a binary star, the observed s-process overabundance could be due to a mass transfer happened in the past, since HD 55496 is not luminous enough to be an AGB star.

4.3 Elemental Abundances

In following Subsections we discuss the abundance pattern of HD 55496 comparing it with previous studies done for some stars in the halo and globular cluster stars, and also with the other chemically peculiar stars where heavy-element overabundances have already been

Table 7. Radial velocity (RV) for HD 55496.

RV (km s ⁻¹)	Ref.
315.63±0.23	1
316.21±0.16	2
315.28±0.80	3
322	4
315.30→317.72	5
317±10	6
317	7

References for Table 7.

- 1: This work;
- 2 GAIA DR2, Bailer-Jones (2018);
- 3: Karinkuzhi & Goswami (2015);
- 4: Gontcharov (2006);
- 5: Jorissen et al. (2005);
- 6: Beers & Sommer-Larsen (1995);
- 7: Luck & Bond (1991);

reported in the literature. Figure 8 shows the abundance pattern of HD 55496 for all the elements analyzed in this work.

4.3.1 Carbon, Nitrogen, Lithium and the ¹²C/¹³C isotopic ratio

As shown in Table 4, the carbon abundance is low compared to a s-process enriched star of similar metallicity such as CD-62°1346, with [Fe/H] = -1.59±0.08 and a [C/Fe] ratio of +0.86 (Pereira et al. 2012). The [N/Fe] ratio is higher than the field giant stars of similar metallicity (Gratton et al. 2000). HD 55496 has a low ¹²C/¹³C ratio (¹²C/¹³C = 6.0±1.0). The high nitrogen abundance and the low ¹²C/¹³C strongly suggest that significant mixing has occurred in the atmosphere of HD 55496. In fact, the [N/Fe] ratio *versus* [Fe/H] of dwarf stars shows no trend in the metallicity range -2.0 < [Fe/H] < +0.3, and [N/Fe] is ≈ 0.0 (Clegg et al. 1981; Tomkin & Lambert 1984; Carbon et al. 1987). As a star becomes a giant, nuclear processed material by the CN cycle which creates more ¹⁴N and more ¹³C relative to ¹²C, due to the deepening of its convective envelope, is brought from the interior to the outer layers of the star changing the surface composition.

The excess of C+N is the difference between the total C+N abundance and the expected primordial value. In non-evolved stars, the abundance of nitrogen scales with the iron abundance that is for metallicities between +0.3 and -2.0, therefore the [N/Fe] ratio is basically zero (Wheeler et al. 1989). For carbon we used the trend between the [C/H] *versus* [Fe/H] from Masseron et al. (2006). In HD 55496, the (C+N) abundance sum shows an enhancement of ~1.1 dex compared to stars with similar metallicity, which is seen in Figure 9 notwithstanding the low carbon abundance. The value of (C+N) means that the

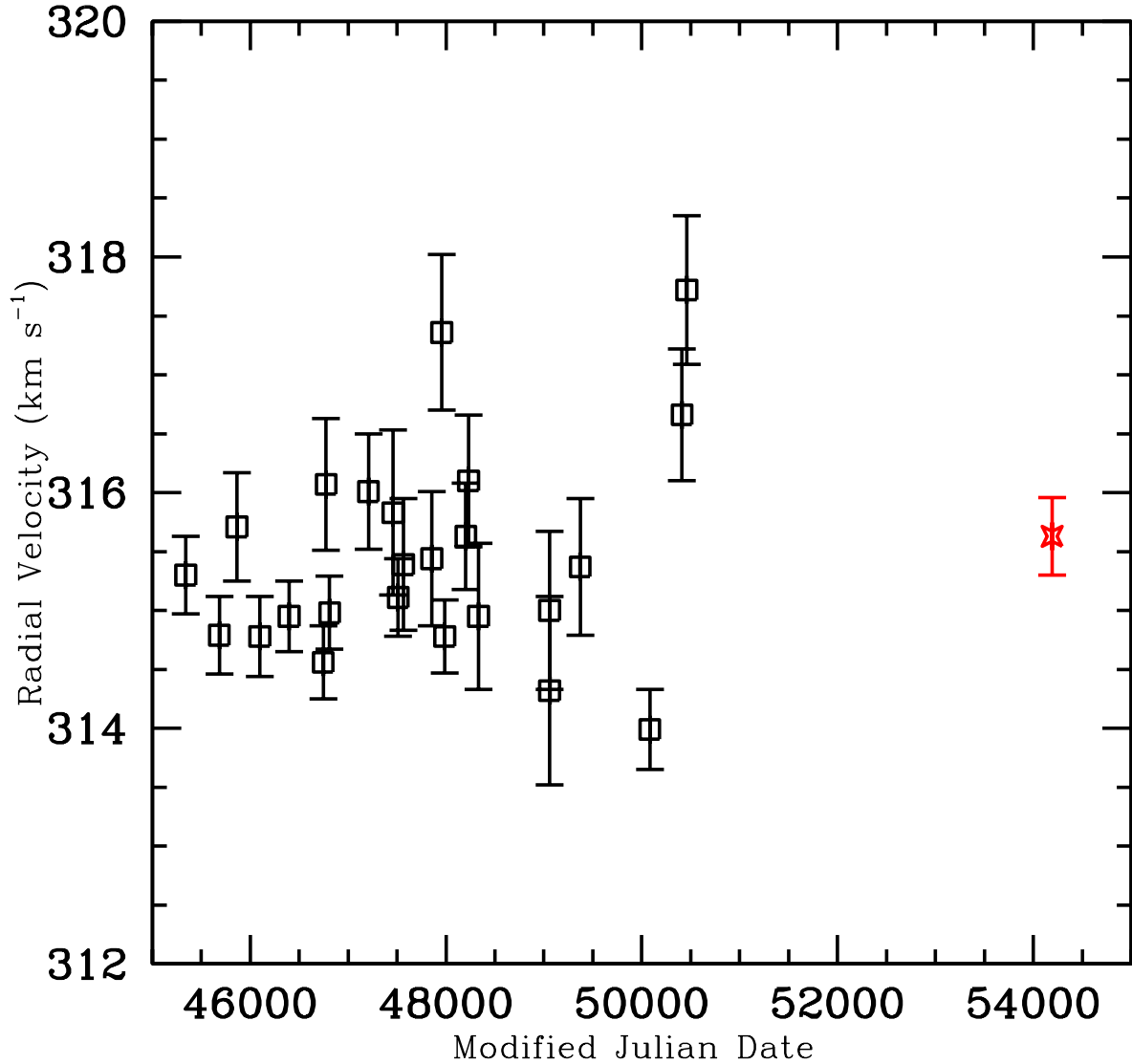


Figure 7. Radial velocity of HD 55496 as a function of the Modified Julian Date (MJD). All data points were taken from Jorissen et al. (2005) (open squares) except the one at MJD = 54194.052 (red star) which was taken by us.

star did not experience the triple-alpha process which would result in the carbon enhanced (see Table 4). Therefore, HD 55496 is not at the AGB phase, a conclusion already obtained in Section 4.1. In addition, the C/O ratio, which is 0.15, gives another evidence that HD 55496 is not carbon enriched.

Nitrogen can be enhanced through two mixing episodes, cool bottom processing (CBP) (Wasserburg et al. 1995)⁴ or hot bottom burning (HBB) (Sackmann & Boothroyd 1992)⁵

⁴ An extra mixing mechanism that takes material from the cool base of the convective zone to the deeper layers of the stellar interior where hydrogen burning occurs.

⁵ Hot Bottom Burning takes place in the stars more massive than $4.0 M_{\odot}$ where the outer convection zone reaches temperatures

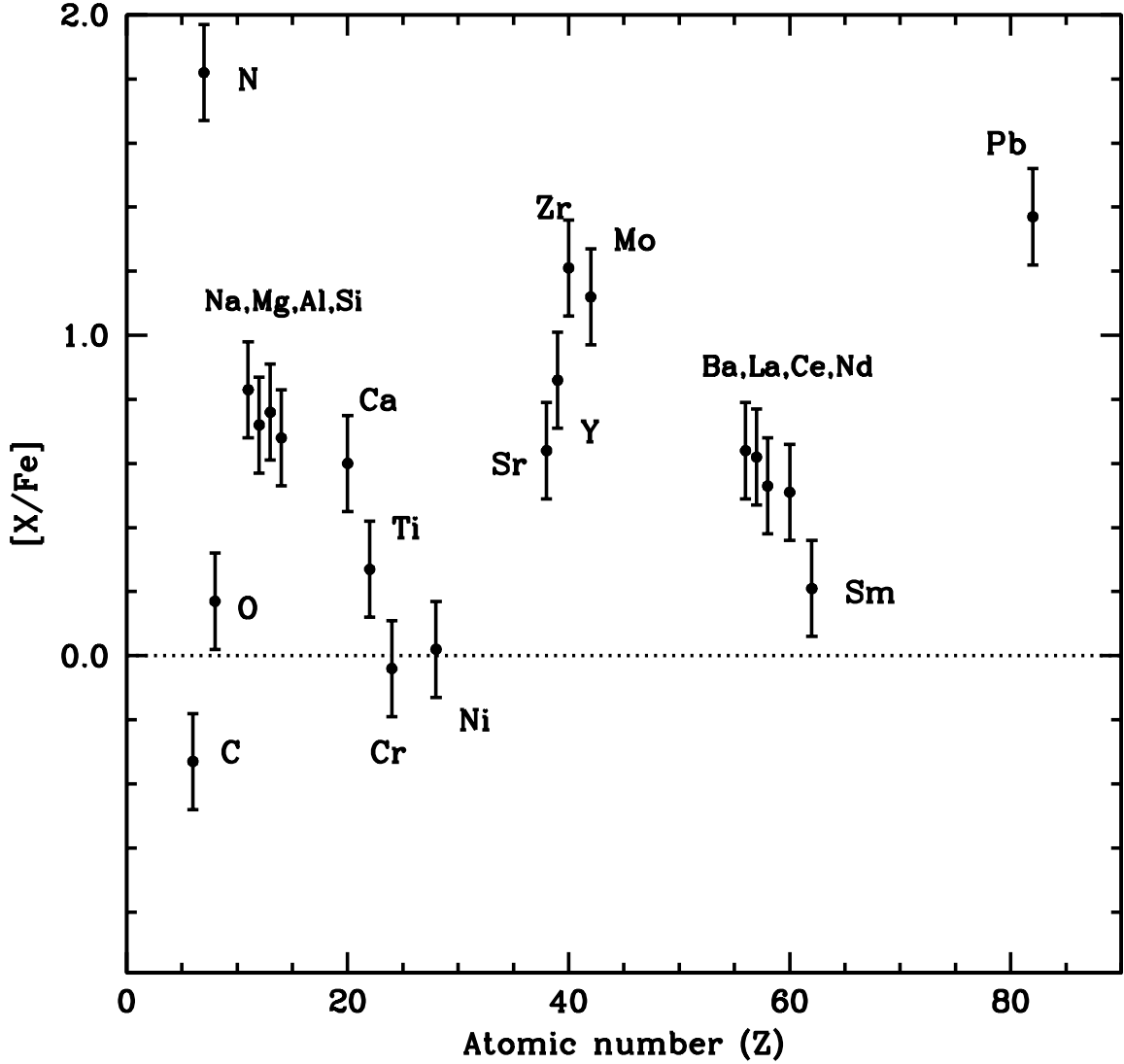


Figure 8. Abundance pattern of HD 55496. The mean elemental abundance is shown versus atomic number

Lithium can also be enhanced thanks to these two mixing process, but as seen in Table 4, lithium is not enhanced. The absence of a high lithium abundance rules out CBP, since Sackmann & Boothroyd (1999) showed that CBP can account for the high lithium abundances. Therefore we should consider HBB as the source of the abundance peculiarities. In Section 4.3.2 we will also provide further support for this conclusion based on the analysis of the abundances of the elements sodium and aluminum.

high enough for proton-capture nucleosynthesis occurring at the base of the outer envelope favoring the conversion of carbon to nitrogen through the CN-cycle.

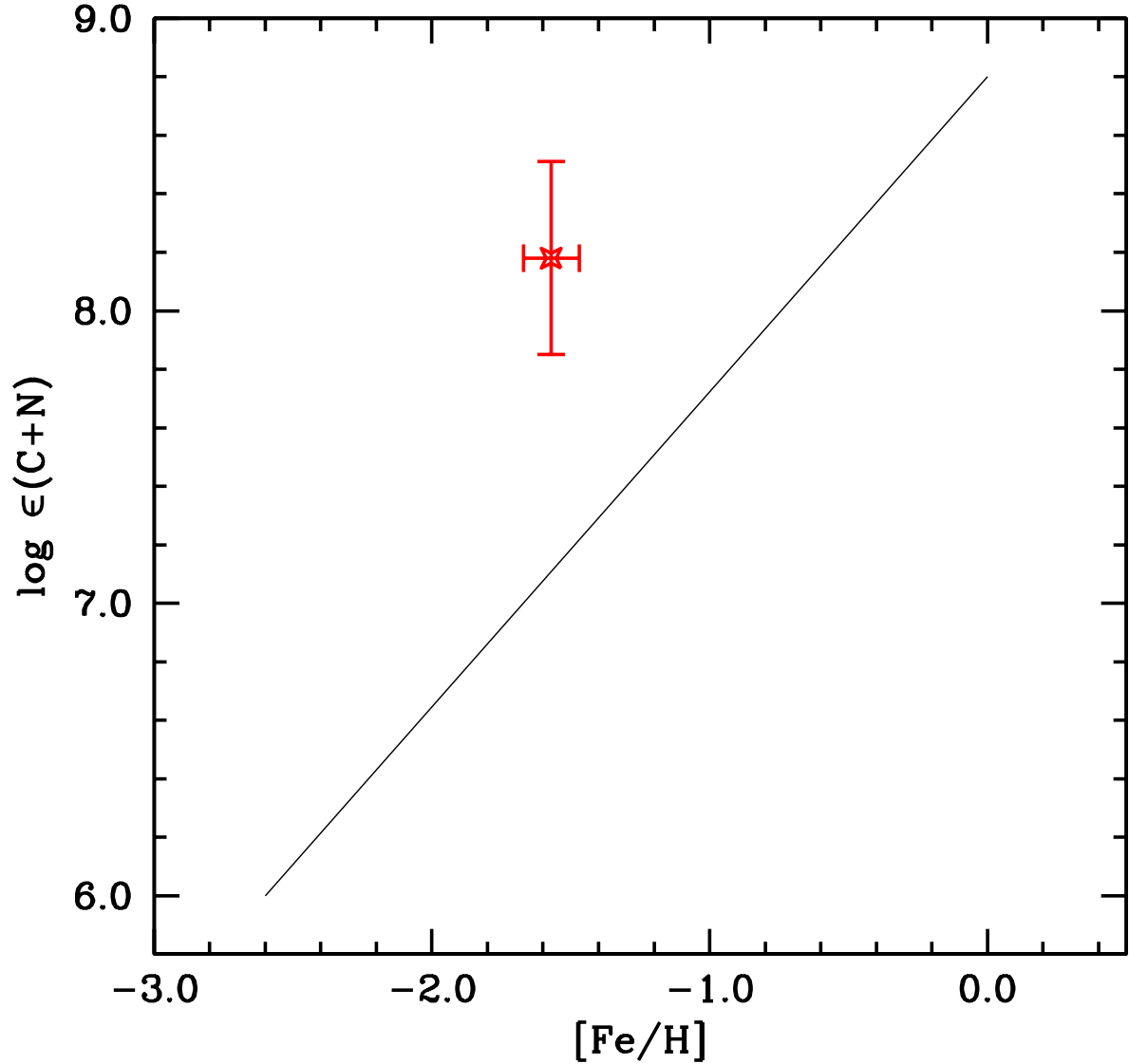


Figure 9. Observed C+N abundance sum in the notation of $\log \epsilon (C+N)$. The solid line shows initial CN abundance for a given metallicity.

4.3.2 Sodium, Aluminum, α - and iron peak elements

In this Section we comment on the abundances of sodium, aluminum elements, alpha-elements and iron-peak elements in comparison with field halo stars and globular cluster stars. Inspecting Table 4, the chemical abundances of HD 55496 present an interesting aspect concerning the abundance of Na and Al. The abundance of these elements is higher compared with field stars of similar metallicity (Norris et al. 2001; Carretta et al. 2010).

In field halo stars with metallicities down to -1.0 , the $[Na/Fe]$ ratio is not higher than $+0.5$ (Timmes et al. 1995). However there are some exceptions, a few stars having $[Na/Fe]$

ratios between +0.6 and +0.7 (Roederer et al. 2014). It is therefore possible that they may represent a population evaporated from globular clusters. The abundance of aluminum ($[Al/Fe]$) in extremely metal-poor stars is never higher than +0.5 (Fullbright 2000; Carretta et al. 2002). Contrary to field stars, both ratios in stars of globular clusters can reach ratios higher than +1.0 (Shetrone 1996; Carretta et al. 2006, just to mention a few references). The $[Na/Fe]$ and $[Al/Fe]$ ratios in HD 54496, with values of +0.83 and +0.76, respectively, are similar to ratios usually observed in globular cluster stars of the "second generation". In addition, the $[O/Fe]$ ratio in HD 55496 is lower than in field stars of similar metallicity. Figure 10 shows the position of HD 55496 in the diagram $[Na/Fe]$ and $[Al/Fe]$ ratios versus the $[O/Fe]$ ratio for some globular cluster stars. Based on the position on these two figures, the most likely explanation for the origin of HD 55496, is that it is an escaped globular cluster star.

As far as the other alpha-elements is concerned, the $[Si/Fe]$, $[Ca/Fe]$, and $[Ti/Fe]$ ratios follow the same trend of halo stars with similar metallicity. The abundances of chromium and nickel follow, as expected, the iron abundance trend. Finally, HD 55496 shows a $[Mg/Fe]$ ratio of +0.72, which is a value previously found in other globular clusters (Gratton et al. 2012; Carretta et al. 2013; Gratton et al. 2014; Gratton et al. 2015).

4.3.3 The *s*-process elements

One of the most interesting aspects of the abundance pattern of HD 55496 for a star to be considered as a "escaped globular cluster star" is the abundance of the *s*-process elements. From Table 4, it is evident that the *light s*-process elements (Sr, Y, Zr, and Mo) show a very high abundance, with a mean of $[ls/Fe] = 0.96 \pm 0.26$. The abundances of the *heavy s*-process elements, given by Ba, La, Ce and Nd, provide a lower $[hs/Fe]$ ratio, which is 0.46 ± 0.14 , therefore the $[hs/ls]$ ratio is -0.50 ± 0.30 . A similar $[hs/ls]$ ratio of -0.35 was obtained by Karinkuzhi & Goswami (2015) for HD 55496. In addition, the $[s/Fe]$ ratio ('s' represents the mean abundance of the *s*-process elements Sr, Y, Zr, Mo, Ba, La, Ce and Pb) is $+0.80 \pm 0.28$. This explains why HD 55496 was previously classified as a barium star by several authors (MacConnell et al. 1972; Bond 1974; Catchpole et al. 1977; Lu et al. 1979; Sneden 1983; Luck & Bond 1991; Karinkuzhi & Goswami 2015).

According to model predictions by Busso et al (2001), for metallicities between -0.5 and -2.0 for a $1.5 M_{\odot}$ AGB star and for metallicities between -0.5 and -1.0 for a $3.0 M_{\odot}$ AGB

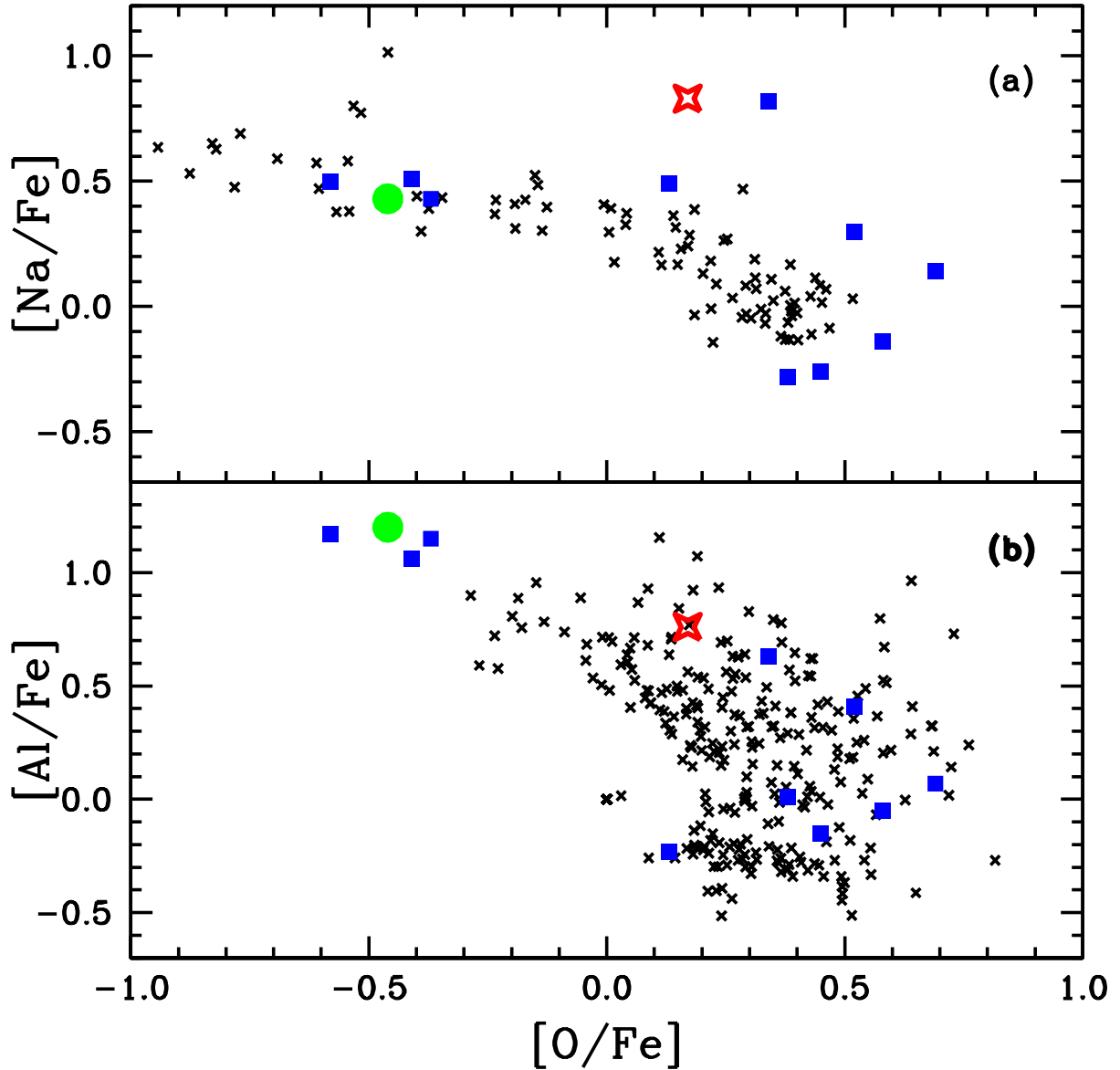


Figure 10. Position of HD 55496 (red star) in the $[Na/Fe]$ ratio versus $[O/Fe]$ ratio diagram (a) and in the $[Al/Fe]$ ratio versus $[O/Fe]$ ratio diagram (b), compared to the position TYC 5691-109-1 (green circle, analyzed by Pereira et al. 2017) and also compared to the position of stars of other globular clusters. Data were taken from: (i) Carretta et al. (2006) for the $[Na/Fe]$ and $[O/Fe]$ ratios in NGC 2808 (black crosses); (ii) Fernández-Trincado et al. (2016) for several globular clusters for the $[Al/Fe]$ and $[O/Fe]$ ratios (black crosses) based on DR13 from APOGEE and (iii) Smith et al. (2000) for the ω Cen (blue squares).

star the $[hs/ls]$ ratio has a maximum value around ≈ 1.2 , which means that heavy s-process elements are the dominant products of neutron capture in AGB stars at those metallicities lower than solar. In AGB stars at near solar metallicities, the light s-process elements are the dominant products of neutron capture. Therefore the index $[hs/ls]$ is an important measure of the neutron capture efficiency and has been widely used in the AGB nucleosynthesis models. This anti-correlation between the $[hs/ls]$ versus metallicity is due to the operation

of the $^{13}\text{C}(\alpha, n)^{16}\text{O}$ reaction, as this neutron source is anti-correlated with the metallicity (Wallerstein 1997).

Negative [hs/ls] indexes are also predicted by models of Busso et al. (2001) for stars with $-2.0 \leq [\text{Fe}/\text{H}] \leq -1.0$ however, none of the chemically peculiar binary stars where the overabundances of the elements created by the s-process are due to a mass-transfer during the AGB phase of the primary star, have negative [hs/ls] index at the same metallicity of HD 55496. This is shown in Figure 11 where the values of the [hs/ls] index for barium stars, CH stars⁶ and CEMP-s stars are displayed. HD 55496 falls in a different position compared to the other chemically peculiar binary stars, which is below the main trend of the anti-correlation between the [hs/ls] and [Fe/H]. This may raise the possibility that other enrichment processes, rather than the mass transfer hypothesis, were responsible for the overabundance in light s-process elements observed in HD55496. Another evidence that can probably rule out the hypothesis of mass-transfer is due to the inconclusive results of the behavior of the radial velocity (Section 4.2), not permitting to confirm or reject a binary nature of HD 55496. In addition, as seen in Section 4.1, we may disregard self-enrichment of HD 55496 in s-process elements because of its low luminosity to be considered an AGB star. Therefore, we suggest as the most probable explanation that the observed overabundance of the light s-process elements was due to the s-process enriched medium where HD 55496 was born and where AGB stars have played a dominant role in the chemical evolution.

In order to verify this possibility we should search among the AGB models those that predict negative [hs/ls] index for low metallicity. Models of massive AGB stars between 5.0 and 8.0 M_{\odot} predict negative [hs/ls] ratios considering the reaction $^{22}\text{Ne}(\alpha, n)^{25}\text{Mg}$ as the most likely neutron source for the origin of the s-process elements (Karakas & Lattanzio 2014; Cristallo et al. 2015). In Figure 12 we show the position of HD 55496 in the diagrams [hs/ls] and [Pb/hs] versus iron abundance together with AGB model predictions given by Cristallo et al. (2015) for AGB stars between 4.0 and 6.0 M_{\odot} at $[\text{Fe}/\text{H}] < -1.0$. It is clear that based on the position of HD 55496 in both diagrams, its abundance pattern can be reproduced by an AGB star with 5.0-6.0 M_{\odot} . Therefore, if indeed HD 55496 is a “second generation” escaped globular cluster star, as suggested by the overabundances of sodium and aluminum, it is also possible that intermediate-mass AGB stars between 3.0 and 6.0 M_{\odot}

⁶ Chemically peculiar binary systems enhanced in carbon and s-process elements. CH stars belong to the halo population.

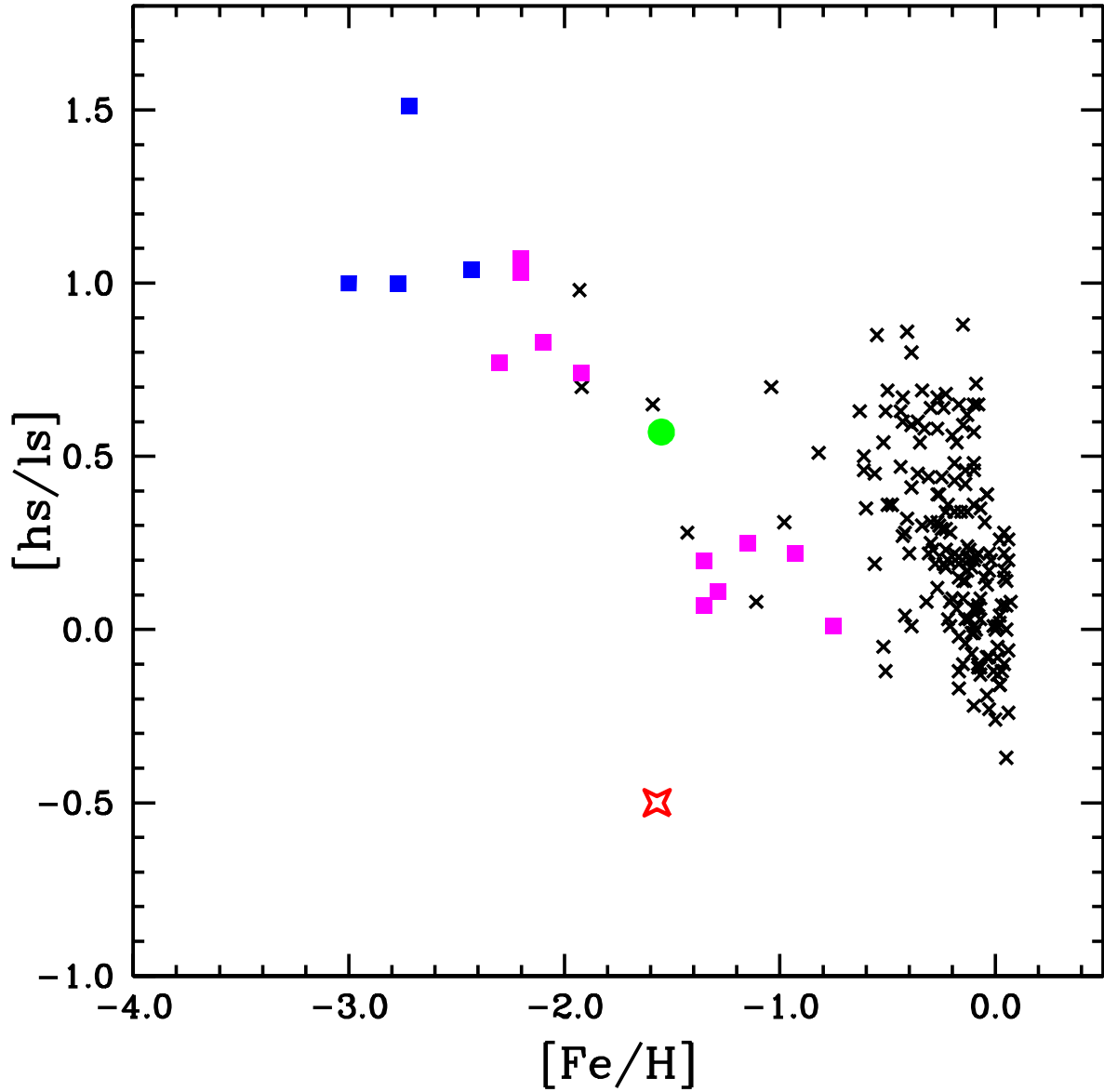


Figure 11. $[hs/ls]$ versus $[Fe/H]$ for HD 55496 (*red star*) and several classes of chemically-peculiar binary stars. Barium giants are represented by *black crosses*, CH stars and yellow symbiotic stars by *magenta squares* and binary CEMP-s stars by *blue squares*. Data for barium stars, CH stars and yellow symbiotic stars were taken from de Castro et al. (2016). Data for binary CEMP-s stars were taken from Preston & Sneden (2001), Sivarani et al. (2004), Barbuy et al. (2005), Lucatello et al. (2003) and Thompson et al. (2008). TYC-5619-109-1 is represented by *green circle*.

were responsible for the production of the elements created by s-process during the time of formation of HD 55496 in a globular cluster.

4.4 Kinematics and Dynamical Origin

In order to investigate whether HD 55496 is a bound or unbound object to the Galaxy and also to investigate the globular cluster origin of HD 55496 we should first not only compare

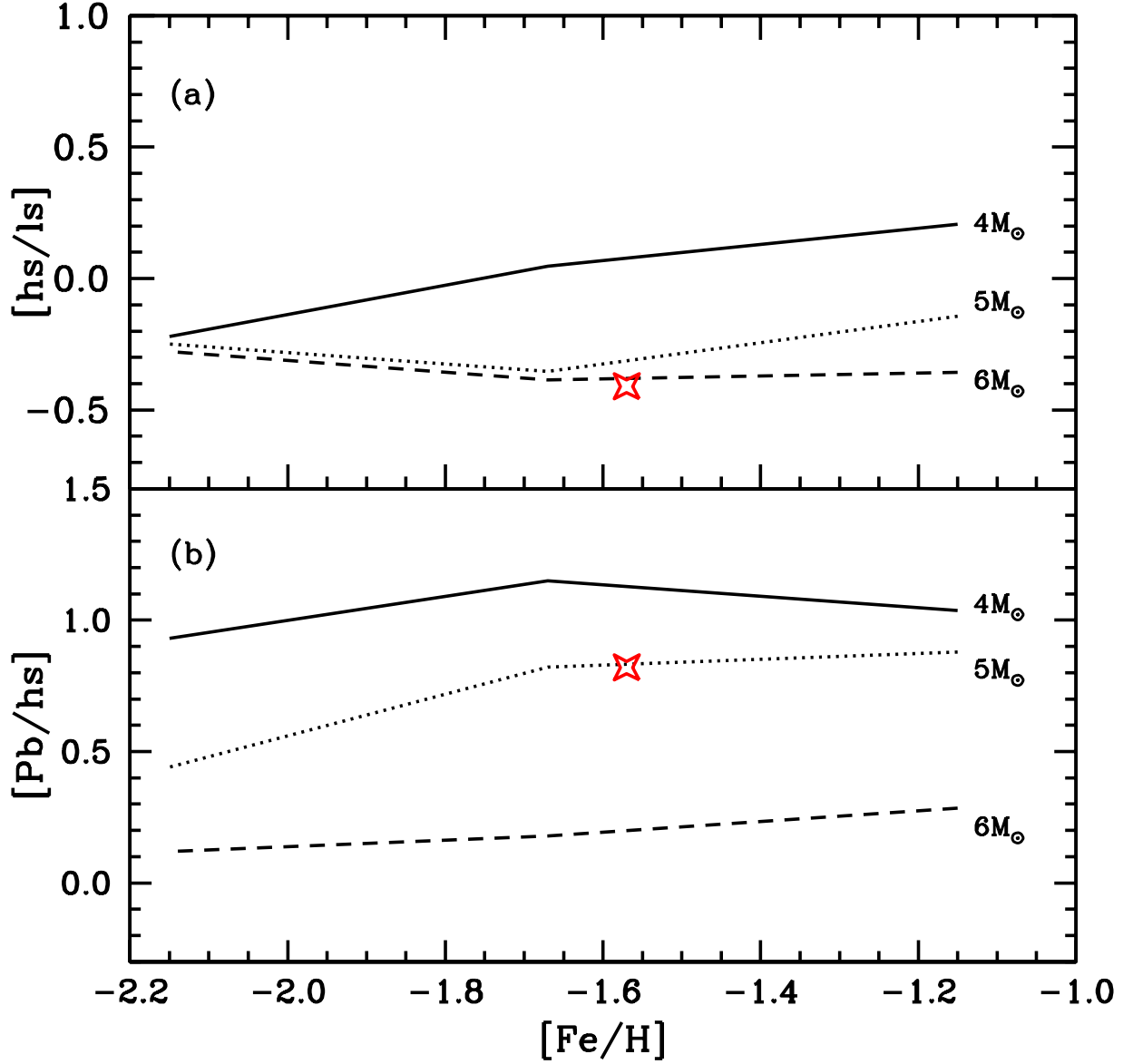


Figure 12. $[\text{hs}/\text{ls}]$ ratio versus $[\text{Fe}/\text{H}]$ (a) and $[\text{Pb}/\text{hs}]$ ratio versus $[\text{Fe}/\text{H}]$ (b) for HD 55496 in comparison with AGB model predictions given by Cristallo et al. (2015) for AGB stars with masses of $4.0 M_{\odot}$, $5.0 M_{\odot}$ and $6.0 M_{\odot}$.

its velocity in the Galactocentric Reference Frame system (V_{GRF}) with the escape Galactic velocity but also to perform a dynamical analysis of its orbital evolution.

Knowing the distance, the proper motion and the radial velocity of HD 55496 we are able to calculate the space velocity components (U_0, V_0, W_0) using the algorithm by Johnson & Soderblom (1987). We also consider the peculiar solar motion of $(8.5, 13.4, 6.5) \text{ km s}^{-1}$, as derived by Coşkunoğlu et al. (2011) and the proper motion of HD 55496 taken from Høg et al (2000). A Galactocentric solar distance of 8.5 kpc and a local standard of rest (LSR) rotation velocity relative to the GRF of 220 km s^{-1} was adopted in our calculations. The

Table 8. Probabilities for HD 55496 to have a close encounter with a globular cluster within a given distance in terms of the cluster tidal radius, r_c . Only the four clusters with the largest probabilities are reported, together with the corresponding average encounter velocities v_{enc} . Cluster iron abundances are from Kharchenko et al. (2013)

Name	$p(< 1.5r_c)$ (%)	$p(< 5r_c)$ (%)	v_{enc} km s^{-1}	[Fe/H]
NGC 5139	6.0	16.2	370 ± 120	-1.445
NGC 6402	4.0	14.8	502 ± 157	-1.145
NGC 6749	4.6	16.3	528 ± 204	-1.600
Terzan 4	3.4	15.3	589 ± 99	-1.045

results for U_0, V_0, W_0 are respectively 130.0 km s^{-1} , -55.3 km s^{-1} and 4.4 km s^{-1} . Considering the uncertainty of 11 pc in the distance (Section 4.1), we obtain a modulus of the star velocity in the GRF of $V_{\text{GRF}} = 141 \pm 0.5 \text{ km s}^{-1}$. This velocity is much lower than the escape Galactic velocity of $V_{\text{esc}} = 532 \text{ km s}^{-1}$, which corresponds to the value provided by the Galactic gravitational potential of Allen & Santillan (1991) at an heliocentric distance of 494 pc. Therefore HD 55496 appears to be a bound object to the Galaxy, however presents $V_0 < 0$, which indicate that is a halo intruder object.

We performed a numerical simulation of the orbit of HD 55496 using a Bulirsh-Stoer integrator that solves the equations of motion of the star in the potential of Allen & Santillan (1991). The star shows a very elongated trajectory, with an eccentricity of $e = 0.84$. It reaches the periastron at 0.87 kpc with a velocity of 477 km s^{-1} , and the apoastron at 10.45 kpc with a velocity of 40 km s^{-1} . In order to check a possible globular cluster origin of this star, we applied the same procedure as in Pereira et al. (2017). The orbit of the star was simulated over 12 Gyr into the past, together with the orbits of 142 globular clusters from the catalog of Kharchenko et al. (2013). During the simulation, we tracked the mutual distances between the star and each cluster, and computed the encounter probabilities within a given distance d . The simulation was repeated 5000 times considering different orbital parameters for the star and the clusters within their 1σ uncertainties. Table 8 summarizes the results for values of d corresponding to 1.5 and 5.0 cluster tidal radii. The low encounter probabilities indicate that the origin of HD 55496 is unlikely to be related to any globular cluster. The few cases displaying the largest probabilities are also associated to very large mutual encounter velocities, indicating that even in such cases the star probably did not detach from the cluster by tidal forces. From the dynamical point of view, HD 55496 has similarities with TYC 5619-109-1 (Pereira et al. 2017), and may represent another example of a possible leftover from a tidally disrupted dwarf galaxy.

5 CONCLUSIONS

Based on high-resolution optical spectroscopic data, we presented a new chemical analysis of HD 55496, a star previously known as barium star. We determined abundances of light elements, Na, Al, alpha-elements, iron-peak elements, and *s*-process elements. We showed that HD 55496 is a metal-poor star characterized by an enhancement of nitrogen, sodium, aluminum and *s*-process elements including lead. The oxygen abundance is low when compared to field metal poor stars of similar metallicity.

Our results show that HD 55496 present a Na–O anti-correlation usually observed among globular cluster stars. The star is also aluminum rich. HD 55496 presents a ratio $[Al/Mg] = +0.04$ which could be classified as a value between to a primordial and intermediate globular cluster populations according to Carretta et al. (2012). But since the $[Al/Fe]$ ratio is $+0.76$, which is a “typical” value for an intermediate population, HD 55496 owed, probably, its abundance pattern due to a different polluters (Carretta et al. 2012).

As was classified as a barium star, HD 55496 is *s*-process enriched but its heavy-element abundance pattern strongly differs from those of the low-metallicity and chemically-peculiar binary stars, in sense that the abundance of Sr, Y and Zr is higher than the abundance of Ba, La, Ce and Nd. In fact, the value of the $[hs/l_s]$ ratio is -0.50 , never observed for a chemically-peculiar binary star at the metallicity of HD 55496. This suggests that the main source of the neutrons is not the $^{13}C(\alpha, n)^{16}O$ reaction but the $^{22}Ne(\alpha, n)^{25}Mg$ reaction. If this is the case, the origin of the heavy-element abundance pattern was provided by stars with masses higher than $4.0 M_{\odot}$, or by the intermediate mass stars which have polluted HD 55496, just like these stars were responsible for the abundances seen among the “second generation of the globular cluster stars”. In the earlier paper (Pereira et al. 2017) we showed that TYC 5619-109-1 presented a chemistry that may have been formed in a globular cluster. In addition, it was also showed that TYC 5619-109-1 is carbon poor and *s*-process enriched. However, HD 55496 differs from TYC 5619-109-1 in sense that the HD 55496 seems to owe its heavy-element abundance pattern due a pollution by massive stars while for TYC 5619-109-1 the contamination may have happened by a mass transfer or by a pollution of a gas already strongly enriched in *s*-process elements. Both HD 55496 and TYC 5619-109-1 are up to now the only two known *s*-process enriched globular cluster escaped stars. Finally, the kinematical and dynamical analysis shows that HD 55496 may have originated from a globular cluster however having a retrograde motion, we can not rule out the possibility that

may have originated from a tidally disrupted dwarf galaxy. The low encounter probabilities with a globular clusters leaves open the origin of HD 55496.

6 ACKNOWLEDGEMENTS

We thank Verne Smith, Simone Daflon and João Victor S. Silva for fruitful discussions. NAD acknowledges Russian Foundation for Basic Research (RFBR) according to the research projects 18-02-00554 and 18-52-06004. Finally we thank the referee for the suggestions and comments that improved the quality of the paper.

REFERENCES

- Allen, C. & Santillan, A., 1991, *RMxAA*, 22, 255
- Allende Prieto, C., Lambert, D.L. & Asplund, M., 2001, *ApJ*, 556, L63
- Alonso, A., Arribas, S. & Martínez-Roger, C. 1999, *A&AS*, 140, 261
- Antipova, L.I., Boyarchuk, A.A., Pakhomov, Yu. V. & Panchuk, V.E., 2004, *ARep*, 48, 597
- Aoki, W., Norris, J.E., Ryan, S.G., Beers, T.C.; Christlieb, N., 2004, *ApJ*, 608, 917
- Bailer-Jones, C.A.L., 2018, *A&A*, 609, 8
- Barbuy, B., Spite, M., Spite, F., Hill, V., Cayrel, R., 2005, *A&A*, 429, 1031
- Beers, T.C. & Sommer-Larsen, J., 1995, *ApJS*, 96, 175
- Bessell, M.S., Castelli, F. & Plez, B., 1998, *A&A*, 333, 231
- Bond, H.E., 1974, *ApJ*, 194, 95
- Busso, M., Gallino, R., Lambert, D.L., Travaglio, C. & Smith, V.V., 2001, *ApJ*, 557, 802
- Carbon, D.F., Barbuy, B., Kraft, R.P., Friel, E.D. & Suntzeff, N.B., 1987, *PASP*, 99, 335
- Carretta, E., Gratton, R., Cohen, J.G., Beers, T.C. & Christlieb, N., 2002, *AJ*, 124, 481
- Carretta, E., Bragaglia, A., Gratton, R.G., Leone, F., Recio-Blanco, A. et al. 2006, *A&A*, 450, 523
- Carretta, E., Bragaglia, A., Gratton, R.G., Recio-Blanco, A. & Lucatello, S. et al., 2010, *A&A*, 516, 55
- Carretta, E., Bragaglia, A., Gratton, R.G., Lucatello, S. & D’Orazi, V., 2012, *ApJ*, 750, L14
- Carretta, E., Gratton, R.G., Bragaglia, A. D’Orazi, V., Lucatello, S. et al., 2013, *ApJ*, 769, 40
- Catchpole, R.M., Robertson, B.S.C. & Warren, P.R., 1987, *MNRAS*, 181, 391
- Cayrel R., 1988, in Cayrel de Strobel G., Spite M., eds, *Proc. IAU Symp.132, The Impact of Very S/N Spectroscopy on Stellar Physics*. Kluwer,Dordrecht, p. 345.
- Chen, B., Vergely, J.L., Valette, B. & Carraro, G., 1998, *A&A*, 336, 137
- Chen, Y.Q., Zhao, G., Nissen, P.E., Bai, G.S. & Qiu, H.M., 2003, *ApJ*, 591, 925
- Clegg, R.E.S., Lambert, D.L. & Tomkin, J., 1981, *ApJ*, 250, 262
- Coşkunoğlu, B., Ak, S., Bilir, S., Karaali, S., Yaz, E., 2011, *MNRAS*, 412, 1237
- Cristallo, S., Straniero, O., Piersanti, L. & Gobrecht, D., 2015, *ApJS*, 219, 40
- Cseh, B., Lugaro, M., D’Orazi, V., de Castro, D.B., Pereira, C.B. et al, 2018, *MNRAS*, 620, 146
- de Castro, D.B., Pereira, C.B., Roig, F., Jilinski, E., Drake, N.A. et al. 2016, *MNRAS*, 459, 4299
- Depagne, E., Hill, V., Spite, M., Spite, F., Plez, B., et al. 2002, *A&A*, 390, 187
- Den Hartog, E.A., Lawler, J.E., Sneden, C. & Cowan, J.J., 2003, *ApJS*, 148, 543
- Drake, J.J. & Smith, G., 1991, *MNRAS*, 250, 89
- Drake, N.A. & Pereira, C.B., 2008, *AJ*, 135, 1070

- Edvardsson, B., Andersen, J., Gustafsson, B., Lambert, D.L., Nissen, P. E., et al. 1993, *A&A*, 275, 101
- Fernández-Trincado, J.G., Robin, A.C., Moreno, E., Schiavon, R.P.; García Pérez, A.E., et al. 2016, *ApJ*, 833, 132
- Fernández-Trincado, Zamora, O., García-Hernández, D.A., Souto, D., Dell’Ágli, F. et al. 2017, *ApJ*, 846, L2.
- Fulbright, J.P., 2000, *AJ*, 120, 1841
- Gontcharov, G.A., 2006, *Ast.Lett*, 32, 759
- Gratton, R.G., Sneden, C., Carretta, E. & Bragaglia, A., 2000, *A&A*, 354, 169
- Gratton, R.G., Villanova, S., Lucatello, S., Sollima, A., Geisler, D., et al. 2012, *A&A*, 544, 12
- Gratton, R.G., Lucatello, S., Sollima, A., Carretta, E., Bragaglia, A. et al. 2014, *A&A*, 563, 13
- Gratton, R. G., Lucatello, S., Sollima, A., Carretta, E., Bragaglia, A. et al. 2015, *A&A*, 573, 92
- Gray, D.F., 1992, *The observation and analysis of stellar photospheres*, Cambridge University Press.
- Grevesse, N. & Sauval, A.J., 1998, *Spa. Sci. Rev.*, 85, 161
- Høg, E., Fabricius, C., Makarov, V.V., Urban, S. & Corbin, T., 2000, *A&A*, 355, L27
- Johnson, D.R.H. & Soderblom, D.R., 1987, *AJ*, 93, 846
- Jorissen, A., Začs, L., Udry, S., Lindgren, H. & Musaev, F.A., 2005, *A&A*, 441, 1135
- Karakas, A.I. & Lattanzio, J.C., 2014, *Publ. Astron. Soc. Australia*, 31, 30
- Karinkuzhi, D. & Goswami, A., 2015, *MNRAS*, 446, 2348
- Karinkuzhi, D., Van Eck, S., Jorissen, A., Goriely, S., Siess, L. et al. 2018, *A&A*, 618, 32
- Kharchenko, N.V., Piskunov, A.E., Schilbach, E., Röser, S. & Scholz, R.-D., 2013, *A&A*, 558, 53
- Kaufer, A., Stahl, O. Tubbesing, S., et al. 1999, *The Messenger*, 95, 8.
- Kurucz, R.L. 1993, CD-ROM 13, *Atlas9 Stellar Atmosphere Programs and 2 km/s Grid* (Cambridge: Smithsonian Astrophys. Obs)
- Lambert, D.L., Heath, J.E., Lemke, M. & Drake, J., 1996, *ApJS*, 103, 183
- Lawler, J.E., Den Hartog, E.A., Sneden, C. & Cowan, J.J., 2006, *ApJS*, 162, 227.
- Lawler, J.E., Sneden, C., Cowan, J.J., Ivans, I.I. & Den Hartog, E.A., 2009, *ApJS*, 182, 51
- Lattanzio, J.C., 1986, *ApJ*, 311, 708
- Ljung, G., Nilsson, H., Asplund, M. & Johansson, S., 2006, *A&A*, 456, 1181
- Lü, P.K. & Sawyer, D., 1979, *ApJ*, 231, 144
- Lucatello, S., Gratton, R., Cohen, J.G., Beers, T.C., Christlieb, N. et al., 2003, *AJ*, 125, 875
- Luck, R.E. & Bond, H.E. 1991, *ApJS*, 77, 515
- MacConnell, D.J., Frye, R.L., Uppgren, A.R., 1972, *AJ*, 77, 384
- McWilliam, A., 1998, *AJ*, 115, 1640
- Majewski, S.R., Nidever, D.L., Smith, V.V., Damke, G.J.; Kunkel, W.E., 2012, *ApJ*, 747, L37
- Martell, S.L., Shetrone, M.D., Lucatello, S., Schiavon, R.P., Mészáros, S., 2016, *ApJ*, 825, 146
- Martin, W. C., Fuhr, J. R., Kelleher, D. E., et al. 2002, *NIST Atomic Spectra Database* (Version 2.0; Gaithersburg, MD: NIST)
- Masseron, T., van Eck, S., Famaey, B., Goriely, S., Plez, B. & Siess, L., 2006, *A&A*, 455, 1059
- Norris, J.E., Ryan, S.G. & Beers, T.C., 2001, *ApJ*, 561, 1043
- Pereira, C.B. & Drake, N.A., 2009, *A&A*, 496, 791
- Pereira, C.B., Jilinski, E., Drake, N.A., de Castro, D.B., Ortega, V.G., 2012, *A&A*, 543, 58
- Pereira, C.B., Smith, V. V., Drake, N. A., Roig, F., Hasselquist, S., Cunha, K. et al., 2017, *MNRAS*, 469, 774
- Pereira, C.B., Holanda, N., Drake, N.A. & F.Roig, 2019, *AJ*, 157, 70.
- Preston, G.W. & Sneden, C., 2001, *ApJ*, 122, 1545
- Ramírez, I., Meléndez, J. & Chanamé, J., 2012, *ApJ*, 757, 164
- Reddy, B. E., Bakker, E. J. & Hrivnak, B.J. 1999, *ApJ*, 524, 831
- Reddy, B.E., Tomkin, J., Lambert, D.L. & Allende Prieto, C., 2003, *MNRAS*, 340, 304
- Roederer, I.U., Preston, G.W., Thompson, I.B., Shectman, S.A. & Sneden, C., et al. 2014, *AJ*, 147, 136

- Roederer, I.U. & Thompson, I.B., 2015, MNRAS, 449, 3889
- Roriz, M., Pereira, C.B., Drake, N.A., Roig, F. & Sales Silva, J.V., 2017, A&A, 472, 350
- Sackmann, I.-J. & Boothroyd, A.I., 1992, ApJ, 392, 71
- Sackmann, I.-J. & Boothroyd, A.I., 1999, ApJ, 510, 217
- Santrich, O.J.K., Pereira, C.B. & Drake, N.A., 2013, A&A, 554, A2
- Schiavon, R.P., Zamora, O., Carrera, R., Lucatello, S., Robin, A.C. et al, 2017, MNRAS, 465, 501
- Shetrone, M.D., 1996, AJ, 112, 1517.
- Sivarani, T., Bonifacio, P., Molaro, P., Cayrel, R., Spite, M., 2004, A&A, 413, 1073
- Smith, G., Edvardsson, B. & Frisk, U., 1986, A&A, 165, 126
- Smith, V.V., Suntzeff, N.B., Cunha, K., Gallino, R.; Busso, M., et al. 2000, AJ, 119, 1239
- Smith, V.V., Cunha, K., Jorissen, A. & Boffin, H.M.J. 1996, A&A, 315, 179
- Sneden, C., 1973, Ph.D. Thesis, Univ. of Texas
- Sneden, C., 1983, PASP, 95, 745
- Sneden, C., McWilliam, A., Preston, G.W., Cowan, J.J., Burris, D.L. & Armosky, B.J., 1996, ApJ, 467, 819
- Sobeck, J.S., Lawler, J.E. & Sneden, C., 2007, ApJ, 667, 1267
- Takeda, Y. & Takada-Hidai, M., 1994, PASJ, 46, 395
- Tautvaišienė, G., Edvardsson, B. & Puzeras, E., 2010, MNRAS, 409, 1213.
- Thompson, I.B., Ivans, I.I., Bisterzo, S., Sneden, C., Gallino, R., 2018, 2008, ApJ, 677, 556
- Timmes, F.X., Woosley, S.E. & Weaver, T.A., 1995, ApJS, 98, 617
- Tomkin, J. & Lambert, D.L., 1984, PASP, 96, 226
- van Eck, S., Goriely, S., Jorissen, A. & Plez, B., 2003, A&A, 404, 291
- Vassiliadis, E. & Wood, P.R., 1993, ApJ, 413, 641
- Wallerstein, G., 1997, RvMP, 69, 995
- Wasserburg, G.J., Boothroyd, Arnold I. & Sackmann, I.-J., 1995, ApJ, 447, L37
- Wheeler, J.C., Sneden, C., & Truran, J.W., 1989, ARA&A, 27, 279
- Wood, M.P., Lawler, J.E., Sneden, C. & Cowan, J.J., 2014, ApJS, 211, 20
- Wiese, W. L., Smith, M. W. & Miles, B. M. 1969, NBS Ref. Data. Ser.
- Yong, D., Norris, J.E., Da Costa, G.S., Stanford, L.M., Karakas, A.I., 2017, ApJ, 837, 176

This paper has been typeset from a $\text{\TeX}/\text{\LaTeX}$ file prepared by the author.

Table 1. Observed Fe I and Fe II lines

Element	$\lambda(\text{\AA})$	$\chi(\text{eV})$	$\log gf$	$W_\lambda(\text{m\AA})$
Fe I	5133.69	4.18	0.20	89
	5150.84	0.99	-3.00	114
	5151.91	1.01	-3.32	106
	5159.06	4.28	-0.65	30
	5162.27	4.18	0.07	82
	5194.94	1.56	-2.09	123
	5198.71	2.22	-2.14	87
	5232.94	2.94	-0.08	139
	5242.49	3.63	-0.97	58
	5250.21	0.12	-4.92	85
	5281.79	3.04	-0.83	101
	5302.31	3.28	-0.74	90
	5307.36	1.61	-2.97	84
	5322.04	2.28	-2.84	43
	5339.93	3.27	-0.68	95
	5341.02	1.61	-1.95	135
	5364.87	4.45	0.23	71
	5367.47	4.42	0.43	75
	5369.96	4.37	0.54	82
	5373.71	4.47	-0.71	22
	5393.17	3.24	-0.72	91
	5400.50	4.37	-0.10	59
	5410.91	4.47	0.40	71
	5445.04	4.39	0.04	62
	5487.75	4.32	-0.65	43
	5506.78	0.99	-2.80	130
	5522.45	4.21	-1.40	14
	5554.90	4.55	-0.38	41
	5560.21	4.43	-1.04	15
	5563.60	4.19	-0.84	46
	5567.39	2.61	-2.56	38
	5569.62	3.42	-0.49	95
	5572.84	3.40	-0.28	104
	5576.09	3.43	-0.85	76
	5624.02	4.39	-1.33	12
	5686.53	4.55	-0.45	26
	5691.50	4.30	-1.37	10
	5717.83	4.28	-0.97	25
	5731.76	4.26	-1.15	22
	5762.99	4.21	-0.41	58
	5791.02	3.21	-2.27	36
	5883.82	3.96	-1.21	34
	5916.25	2.45	-2.99	37
	6024.06	4.55	-0.06	53
	6027.05	4.08	-1.09	29
	6056.01	4.73	-0.40	25
	6065.48	2.61	-1.53	106
	6079.01	4.65	-0.97	25
	6136.61	2.45	-1.40	115
	6137.69	2.59	-1.40	107
	6151.62	2.18	-3.29	31
	6157.73	4.08	-1.11	36
	6170.51	4.79	-0.38	28
	6173.34	2.22	-2.88	59
	6191.56	2.43	-1.42	114
	6200.31	2.60	-2.44	51
	6213.43	2.22	-2.48	74
	6230.72	2.56	-1.28	121
	6252.56	2.40	-1.72	107
	6265.13	2.18	-2.55	85
	6322.69	2.59	-2.43	59
	6393.60	2.43	-1.43	120
	6411.65	3.65	-0.66	82
	6419.95	4.73	-0.09	41
	6421.35	2.28	-2.01	100
	6430.85	2.18	-2.01	108
	6592.91	2.72	-1.47	93
	6593.87	2.44	-2.42	68

Table 1, continued

Element	$\lambda(\text{\AA})$	$\chi(\text{eV})$	$\log gf$	$W_\lambda(\text{m\AA})$
	6609.11	2.56	-2.69	49
	6750.15	2.42	-2.62	69
Fe II	4993.35	2.81	-3.67	26
	5132.66	2.81	-4.00	12
	5197.56	3.23	-2.25	66
	5284.10	2.89	-3.01	43
	5325.56	3.22	-3.17	24
	5414.05	3.22	-3.62	15
	5425.25	3.20	-3.21	26
	5534.83	3.25	-2.77	40
	6084.10	3.20	-3.80	11
	6432.68	2.89	-3.58	29

Table 3. Other lines studied

$\lambda(\text{\AA})$	Element	$\chi(\text{eV})$	$\log gf$	Ref	$W_\lambda(\text{m\AA})$
4664.81	Na I	2.10	-1.55	T94	28
4668.60	Na I	2.10	-1.30	T94	29
4982.81	Na I	2.10	-0.95	T94	54
5682.65	Na I	2.10	-0.70	T94	77
5688.22	Na I	2.10	-0.37	T94	97
6154.22	Na I	2.10	-1.51	T94	23
6160.75	Na I	2.10	-1.21	T94	40
8183.26	Na I	2.10	+0.22	T94	168
4702.99	Mg I	4.35	-0.52	A2004	146
4730.04	Mg I	4.34	-2.39	R03	35
5528.40	Mg I	4.35	-0.49	A2004	157
5711.10	Mg I	4.34	-1.68	R99	78
8736.04	Mg I	5.94	-0.34	WSM	82
6696.03	Al I	3.14	-1.48	MR94	18
6698.67	Al I	3.14	-1.63	R03	17
7835.32	Al I	4.02	-0.58	R03	28
7836.13	Al I	4.02	-0.40	R03	25
8772.88	Al I	4.02	-0.25	R03	41
8773.91	Al I	4.02	-0.07	R03	59
5793.08	Si I	4.93	-2.06	R03	46
6125.03	Si I	5.61	-1.54	E93	15
6131.58	Si I	5.62	-1.69	C2003	10
6145.08	Si I	5.62	-1.43	E93	43
7800.00	Si I	6.18	-0.72	E93	27
8742.45	Si I	5.87	-0.51	E93	65
5581.80	Ca I	2.52	-0.67	C2003	76
5601.29	Ca I	2.52	-0.52	C2003	77
5857.46	Ca I	2.93	+0.11	C2003	99
6102.73	Ca I	1.88	-0.79	D2002	113
6122.23	Ca I	1.89	-0.32	D2002	142
6166.44	Ca I	2.52	-1.14	R03	48
6169.04	Ca I	2.52	-0.80	R03	74
6169.56	Ca I	2.53	-0.48	DS91	88
6439.08	Ca I	2.52	+0.47	D2002	137
6449.82	Ca I	2.52	-0.50	C2003	85
6455.60	Ca I	2.51	-1.29	R03	40
6464.68	Ca I	2.52	-2.41	C2003	13
6471.66	Ca I	2.51	-0.69	S86	78
6493.79	Ca I	2.52	-0.11	DS91	113
6499.65	Ca I	2.52	-0.81	C2003	72
6717.69	Ca I	2.71	-0.52	C2003	84

$\lambda(\text{\AA})$	Element	$\chi(\text{eV})$	$\log gf$	Ref	$W_\lambda(\text{m\AA})$
4758.12	Ti I	2.25	+0.43	MFK	29
4759.28	Ti I	2.25	+0.51	MFK	32
4981.74	Ti I	0.85	+0.50	D2002	115
4997.10	Ti I	0.00	-2.12	MFK	48
5009.66	Ti I	0.02	-2.26	MFK	35
5016.17	Ti I	0.85	-0.57	MFK	75
5022.87	Ti I	0.83	-0.43	MFK	79
5039.96	Ti I	0.02	-1.13	MFK	94
5043.59	Ti I	0.84	-1.73	MFK	16
5087.06	Ti I	1.43	-0.84	E93	22
5145.47	Ti I	1.46	-0.57	MFK	29
5147.48	Ti I	0.00	-2.01	MFK	52
5152.19	Ti I	0.02	-2.02	MFK	51
5210.39	Ti I	0.05	-0.88	MFK	108
5219.71	Ti I	0.02	-2.29	MFK	34
5295.78	Ti I	1.05	-1.63	MFK	14
5490.16	Ti I	1.46	-0.94	MFK	18
5866.46	Ti I	1.07	-0.87	E93	51
5922.12	Ti I	1.05	-1.47	MFK	22
5978.55	Ti I	1.87	-0.50	MFK	20
6126.22	Ti I	1.05	-1.37	R03	22
6258.11	Ti I	1.44	-0.36	MFK	47
6261.10	Ti I	1.43	-0.48	MFK	41
6554.24	Ti I	1.44	-1.22	MFK	18
4789.34	Cr I	2.54	-0.33	S07	44
4829.37	Cr I	2.54	-0.51	S07	21
4870.80	Cr I	3.08	-0.01	S07	29
5296.70	Cr I	0.98	-1.36	S07	76
5298.28	Cr I	0.98	-1.14	S07	87
5345.81	Cr I	1.00	-0.95	S07	97
5409.79	Cr I	1.03	-0.67	S07	109
5783.87	Cr I	3.32	-0.29	S07	10
5787.93	Cr I	3.32	-0.08	S07	11
6330.10	Cr I	0.94	-2.92	S07	14
4519.98	Ni I	1.68	-3.08	W2014	22
4604.99	Ni I	3.48	-0.24	W2014	51
4715.76	Ni I	3.54	-0.33	W2014	42
4756.52	Ni I	3.48	-0.27	W2014	46
4866.27	Ni I	3.54	-0.22	W2014	48
4953.21	Ni I	3.74	-0.58	W2014	26
4976.33	Ni I	1.68	-3.00	W2014	27
5003.75	Ni I	1.68	-3.07	W2014	24
5010.94	Ni I	3.63	-0.98	W2014	21
5017.58	Ni I	3.54	-0.03	W2014	56
5035.36	Ni I	3.64	+0.29	W2014	64
5084.10	Ni I	3.68	-0.18	W2014	51
5102.97	Ni I	1.68	-2.87	W2014	32
5115.40	Ni I	3.83	-0.28	W2014	38
5424.65	Ni I	1.95	-2.74	W2014	26
5435.86	Ni I	1.99	-2.58	W2014	35

Table 3, continued

Table 3, continued

$\lambda(\text{\AA})$	Element	$\chi(\text{eV})$	$\log gf$	Ref	$W_\lambda(\text{m\AA})$
5578.73	Ni I	1.68	-2.67	W2014	43
5587.87	Ni I	1.94	-2.39	W2014	42
5592.26	Ni I	1.95	-2.51	W2014	44
5709.56	Ni I	1.68	-2.30	W2014	73
5748.36	Ni I	1.68	-3.24	W2014	19
5846.99	Ni I	1.68	-3.46	W2014	16
5892.87	Ni I	1.99	-2.22	W2014	58
6007.31	Ni I	1.68	-3.40	W2014	13
6108.12	Ni I	1.68	-2.49	W2014	54
6128.98	Ni I	1.68	-3.32	W2014	18
6176.82	Ni I	4.09	-0.26	W2014	23
6177.25	Ni I	1.83	-3.51	W2014	10
6327.60	Ni I	1.68	-3.15	W2014	29
6482.80	Ni I	1.94	-2.63	W2014	29
6532.88	Ni I	1.94	-3.39	W2014	11
6586.33	Ni I	1.95	-2.81	W2014	24
6643.64	Ni I	1.68	-2.03	W2014	86
6767.77	Ni I	1.83	-2.17	W2014	72
6772.32	Ni I	3.66	-0.97	W2014	17
7788.93	Ni I	1.95	-2.18	W2014	75
4607.33	Sr I	0.00	+0.28	SN96	70
4883.68	Y II	1.08	+0.07	SN96	105
5087.43	Y II	1.08	-0.17	SN96	94
5123.21	Y II	0.99	-0.93	SN96	71
5200.41	Y II	0.99	-0.57	SN96	82
5205.72	Y II	1.03	-0.34	SN96	101
5289.81	Y II	1.03	-1.85	VWR	24
5402.78	Y II	1.84	-0.44	R03	38
4772.30	Zr I	0.62	-0.06	A04	24
4815.05	Zr I	0.65	-0.38	A04	21
5385.13	Zr I	0.52	-0.64	A04	11
6127.46	Zr I	0.15	-1.06	S96	15
6134.57	Zr I	0.00	-1.28	S96	12
6143.18	Zr I	0.07	-1.10	S96	19
4050.32	Zr II	0.71	-1.06	L2006	79
4442.99	Zr II	1.49	-0.42	L2006	69
5112.27	Zr II	1.66	-0.85	L2006	47
5350.35	Zr II	1.77	-1.16	L2006	31
5570.44	Mo I	1.34	-0.34	Y2017	10
4086.71	La II	0.00	-0.16	SN96	79
5880.63	La II	0.24	-1.83	VWR	15
6774.33	La II	0.12	-1.71	VWR	18

Table 3, continued

$\lambda(\text{\AA})$	Element	$\chi(\text{eV})$	$\log gf$	Ref	$W_\lambda(\text{m\AA})$
4418.79	Ce II	0.86	+0.27	L09	41
4483.90	Ce II	0.86	+0.10	L09	29
4486.91	Ce II	0.29	-0.18	L09	39
4539.74	Ce II	0.33	-0.08	L09	49
4562.37	Ce II	0.48	+0.21	L09	59
4628.16	Ce II	0.52	+0.14	L09	52
5187.45	Ce II	1.21	+0.17	L09	17
5274.24	Ce II	1.04	+0.13	L09	26
5330.58	Ce II	0.87	-0.40	L09	11
5393.39	Ce II	1.10	-0.06	L09	14
4462.98	Nd II	0.56	+0.04	DH	53
4706.54	Nd II	0.00	-0.71	DH	39
4709.72	Nd II	0.18	-0.97	DH	26
4715.59	Nd II	0.20	-0.90	DH	17
4797.15	Nd II	0.56	-0.69	DH	13
4825.48	Nd II	0.18	-0.42	DH	44
4859.03	Nd II	0.32	-0.44	DH	38
4902.04	Nd II	0.06	-1.34	DH	15
4914.38	Nd II	0.38	-0.70	DH	20
4959.12	Nd II	0.06	-0.80	DH	31
5092.80	Nd II	0.38	-0.61	DH	26
5130.59	Nd II	1.30	+0.45	DH	25
5165.13	Nd II	0.68	-0.74	DH	15
5212.36	Nd II	0.20	-0.96	DH	21
5234.19	Nd II	0.55	-0.51	DH	22
5249.58	Nd II	0.98	+0.20	DH	30
5255.51	Nd II	0.20	-0.67	DH	35
5293.16	Nd II	0.82	+0.10	DH	28
5311.46	Nd II	0.98	-0.42	DH	12
5319.81	Nd II	0.55	-0.14	DH	37
5485.70	Nd II	1.26	-0.12	DH	13
4318.94	Sm II	0.28	-0.25	L06	27
4424.32	Sm II	0.48	0.14	L06	36
4467.34	Sm II	0.66	0.15	L06	21
4642.23	Sm II	0.38	-0.46	L06	16
4676.90	Sm II	0.04	-0.87	L06	14
4704.40	Sm II	0.00	-0.86	L06	17

References : A2004 : Aoki et al. (2004); A04: Antipova et al. (2004);
 C2003: Chen et al. (2003); D2002: Depagne et al. (2002);
 DH: Den Hartog et al. (2003); DS91: Drake & Smith (1991);
 E93: Edvardsson et al. (2003); L06: Lawler et al. (2006);
 L2006: Ljung et al. (2006); L09: Lawler et al. (2009);
 MFK : Martin et al. (2002); R03: Reddy et al. (2003);
 R99: Reddy et al. (1999); S86: Smith et al. (1986);
 S96: Smith et al. (1996); SN96: Sneden et al. (1996);
 S07: Sobeck et al. (2007); T94: Takeda & Takada-Hidai (1994);
 WSM: Wiese, Smith & Miles (1969); W2014: Wood et al. (2014);
 Y2017: Yong et al. (2017);